Annu. Rev. Phys. Chem. 1999. 50:443–84

HCP ↔ CPH ISOMERIZATION: Caught in the Act

H. Ishikawa,[1] R. W. Field,[2] S. C. Farantos,[3] M. Joyeux,[4] J. Koput,[5] C. Beck,[6] and R. Schinke[6]

[1]*Department of Chemistry, Graduate School of Science, Tohoku University, Sendai 980-8578, Japan;* [2]*Department of Chemistry, Massachusetts Institute of Technology, Cambridge, Massachusetts 02139;* [3]*Institute of Electronic Structure and Laser Foundation for Research and Technology, Hellas, Greece, and Department of Chemistry, University of Crete, Iraklion 711 10, Crete, Greece;* [4]*Laboratoire de Spectrométrie Physique, Université Joseph Fourier, Grenoble I, BP 87, F-38402 St Martin d'Heres Cedex, France;* [5]*Department of Chemistry, Adam Mickiewicz University, 60-780 Poznan, Poland; and* [6]*Max-Planck-Institut für Strömungsforschung, D-37073 Göttingen, Germany; e-mail: rschink@gwdg.de*

Key Words vibrational spectroscopy, polyads, resonance Hamiltonian, bifurcations, periodic orbits

■ **Abstract** In this overview we discuss the vibrational spectrum of phosphaethyne, HCP, in its electronic ground state, as revealed by complementary experimental and theoretical examinations. The main focus is the evolution of specific spectral patterns from the bottom of the potential well up to excitation energies of approximately 25,000 cm^{-1}, where large-amplitude, isomerization-type motion from H–CP to CP–H is prominent. Distinct structural and dynamical changes, caused by an abrupt transformation from essentially HC bonding to mainly PH bonding, set in around 13,000 cm^{-1}. They reflect saddle-node bifurcations in the classical phase space—a phenomenon well known in the nonlinear dynamics literature—and result in characteristic patterns in the spectrum and the quantum-number dependence of the vibrational fine-structure constants. Two polar opposites are employed to elucidate the spectral patterns: the exact solution of the Schrödinger equation, using an accurate potential energy surface and an effective or resonance Hamiltonian (expressed in a harmonic oscillator basis set and block diagonalized into polyads), which is defined by parameters adjusted to fit either the measured or the calculated vibrational energies. The combination of both approaches—together with classical mechanics and semiclassical analyses—provides a detailed spectroscopic picture of the breaking of one bond and the formation of a new one.

0066-426X/99/1001-0443$08.00

INTRODUCTION

One major objective of molecular spectroscopy is an understanding of the forces that couple the various internal degrees of freedom in a polyatomic molecule (1, 2) and thereby control the flow of energy from one mode to another (intramolecular vibrational energy redistribution) (3–8). The strength of these forces is indirectly manifested through the vibrational-rotational levels, i.e. the eigenenergies of the underlying Hamiltonian. The eigenenergies can be measured in a spectroscopic experiment, and they can be calculated from first principles by solving the Schrödinger equation. The understanding we seek is based on the recognition of specific diagnostic patterns in the spectrum, their interpretation in terms of particular features of the Hamiltonian, and the sometimes qualitative changes of these patterns as the total energy increases. This ambition to understand is distinct from the traditional spectroscopic goal of compiling a more-or-less complete list of all energy levels and of parameterizing these levels and relative intensities to the accuracy of spectroscopic experiments.

In what follows, $Q_1, \ldots, Q_N$ designate a particular set of internal coordinates, with N being the number of degrees of freedom. The interactions between the vibrational modes normally depend markedly on the energy, E. Near the bottom of the potential well, the potential energy surface (PES), $V(Q_1, \ldots, Q_N)$ is well approximated by a sum of one-dimensional potentials, $\widetilde{V}_i(Q_i)$, plus some small coupling terms of the form $Q_i^n Q_j^m$, and the spectrum of energy levels closely resembles the spectrum of a set of uncoupled harmonic oscillators. Because the interoscillator coupling is weak in this low-energy regime and because the density of states is small, the classical as well as quantum dynamics is regular, or predictable. As a result, each state can be assigned, without ambiguity, to a set of quantum numbers $(v_1, \ldots, v_N)$. This assignment can be based on either regular patterns of energy levels (experimentally observable) or nodal patterns in the eigenfunctions (experimentally unobservable).

As the energy increases, the intermode coupling gradually becomes stronger, or in other words, the molecule samples regions of the coordinate space where anharmonic effects become increasingly important. The consequence is that the complexity of the energy spectrum increases, and at the same time, fewer and fewer eigenstates can be assigned in a meaningful manner. Eventually, the intermode coupling is so strong that the dynamics becomes irregular and almost all states lose their distinct identity, i.e. the nodal structures of the wave functions are so irregular that a meaningful counting of nodes, and therefore assignment (or description as a specific mixture of states with simple nodal structures), is impossible (9, 10). For such a case, it has been suggested that the only way to extract information from a spectrum is by statistical analysis of the distribution of nearest-neighbor energy spacings and/or relative intensities (11–14).

The transition from the regular to the irregular regime in polyatomic molecules is gradual rather than abrupt; unassignable wave functions appear already at relatively low energies, whereas perfectly regular-looking wave functions still exist in an energy region where most other states are already unassignable (15). It is this

intermediate energy regime that is most difficult to describe—but therefore most compelling for experimental and theoretical studies (2).

In addition to the gradual and incomplete evolution from regularity to irregularity, distinctive new patterns might appear when the shape of the PES changes significantly in a certain energy region. An example is the isomerization barrier (saddle point) between two stable conformers, as in HCN/CNH (16, 17) or acetylene/vinylidene (18). It is reasonable to surmise that the energy-level pattern must change when the energy is sufficiently high so that the wave functions simultaneously explore the potential wells of both isomers. However, as the example of HCP shows, a true potential barrier is not necessarily required for new effects to arise suddenly; an abrupt change of the slope of the PES may be sufficient. The precise nature of these structural changes in the energy-level spectrum and how they reflect the changes in the bond structure of the molecule is one focus of this article.

The two cornerstones of molecular spectroscopy are the experimental spectrum and the solution of the Schrödinger equation using a global PES (Figure 1). The experimentalist faces two inherent problems. The first concerns the completeness of the measured spectrum. Regardless of the method used [overtone pumping, stimulated emission pumping, etc (2, 19, 20)], because of unfavorable vibrational intensity factors, relatively few vibrational states are observed compared with the totality of all states; normally, one is able to follow only certain regular progressions, with states belonging to other progressions not observable at all (and with those not belonging to regular progressions often not being assignable). The second complication of experimental spectroscopy comes from the fact that the spectrum of energy levels does not directly reveal the underlying quantum mechanical

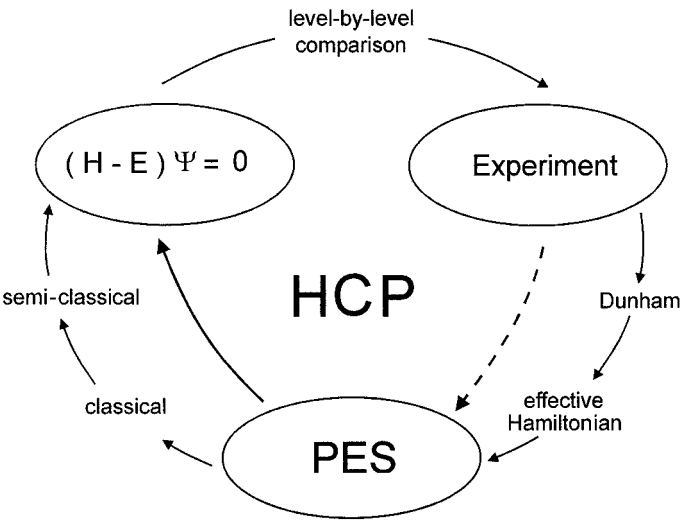

Figure 1 Schematic illustration of how information about the potential energy surface (PES) is obtained from experiment and from theory.

wave functions. At best, the spectrum reflects wave functions only indirectly, through band intensities and rotational and vibrational fine-structure constants. This tremendously complicates the rigorous assigning of the levels, especially at higher energies, where unanticipated changes are likely to occur without warning.

In order to extract information about the PES, the measured spectrum is usually represented by a power series expansion in terms of the quantum numbers v_i (Figure 1). This provides force constants, anharmonic constants, etc. If the spectrum is complicated by an anharmonic resonance effect (accidental or systematic near-degeneracies), the Dunham expansion alone is inappropriate and an effective or resonance model Hamiltonian must be used (21). Such models explicitly take into account approximate constants of motion [such as polyad quantum numbers (22)] and assume particular forms (selection rules and vibrational quantum number scaling) for the elements of the Hamiltonian matrix in a suitable basis. The parameters of the model are then determined by fitting experimental data. Effective Hamiltonian models are known to work very well for a variety of systems. However, a question remains: To what extent are such models applicable when the spectrum significantly changes its behavior, for example, in the vicinity of an isomerization barrier or near a "kink" in the PES, as for HCP?

In the quantum mechanical calculation of the vibrational spectrum, one starts from the PES, solves the Schrödinger equation in a numerically exact way, and compares the calculated energies with the experimental ones (Figure 1). The advantages are the following: All bound-state energies up to the dissociation threshold are obtained, and the full quantum mechanical calculations, in contrast to experiment, also provide the wave functions. This second point is important because without the possibility of examining the nodal structure of the wave functions, assignments become increasingly unreliable at higher energies (23, 24). However, the PES, irrespective of whether it is calculated from first principles or fitted to experimental data, is never the real potential; the calculated and measured energies do not exactly match and the deviations gradually increase with increasing energy. This makes the comparison with the measured spectrum complicated, especially if one examines an energy region where the density of states is large, where unique correspondences between observed and calculated states are a problem, where only a small fraction of the states are seen in the experiment, and where, in addition, some unexpected effects might occur.

Although the exact Hamiltonian method and (approximate) spectroscopic Hamiltonian models start from completely different points, they complement one another. The exact calculations can be used to test the validity and reveal the nature of the eigenstates of spectroscopic Hamiltonians, and vice versa, the model calculations can help to reveal the structure of the exact spectrum, because they are designed in such a way that certain structural elements (e.g. polyads) are explicitly built in. The interplay between the two approaches is another focus of this overview.

Solving the Schrödinger equation yields the exact energies and wave functions—for the particular PES used. However, this enormous body of numerical information offers no guarantee that we will be able to understand the internal vibrational dynamics. In many cases, the analysis of the structure of the

classical phase space has provided extremely valuable insights (25, 26). For example, the backbone of the quantum mechanical wave functions (perpendicular to the pattern of nodal surfaces) often parallels special trajectories, so-called periodic orbits (27). Moreover, the combination of solely classical ingredients with the quantum mechanical superposition principle—called semiclassical mechanics (9, 28)—provides even more detailed insights into the molecular dynamics.

Thus, in order to illuminate the spectrum of a molecule from all perspectives, one needs a highly accurate PES, exact quantum mechanical and effective Hamiltonian calculations, classical and semiclassical calculations, and as much experimental data (both energies and relative intensities) as possible. The experimental data are indispensable to the constructing of a theoretical framework on a solid foundation. We know of no triatomic molecule, besides perhaps water (29, 30), for which all these different facets are available—except for HCP. In this article, we highlight the joint experimental and theoretical efforts made in the past 4 years to assign and interpret the vibrational spectrum of this simple molecule, from very low energies up to the energy range where new and unexpected effects occur. The insight gained from this concerted effort will provide insights into the dynamics of other molecules.

EXPERIMENT

The isomerization of a triatomic monohydride, HAB ↔ ABH, is the simplest example of a bond-breaking isomerization. It is a fundamental cornerstone of molecular dynamics and is addressed in numerous experimental and theoretical studies. One of the key questions—in general as well as in particular for our joint experimental/theoretical investigation of HCP—is how isomerization is encoded into the vibration-rotation spectrum of a HAB molecule, i.e. what is the signature of isomerization on the energy level (and intensity) distribution?

The molecule that has been examined most for signatures of isomerization in the vibrational spectrum is HCN (17, 31). Although there are several extensive experimental studies of highly excited vibrational levels of HCN (32, 33), there is no experimental observation of isomerization states, i.e. states that simultaneously sample both the HCN and the CNH potential wells. As the excited electronic states of HCN, from which highly excited vibrational states in the ground-state manifold can be accessed (see below), lie in the vacuum ultraviolet wavelength region and as most of these states rapidly predissociate, it is difficult to extend the existing spectroscopic experiments to higher energies. The spectroscopic conditions are more favorable for HCP, the third-row homologue of HCN, and as we show below, the symptoms of isomerization indeed can be perceived.

The study of isomerization requires excitation of highly excited bending states, i.e. states that contain large-amplitude motion of the hydrogen atom around the AB entity. High-resolution direct absorption spectroscopic methods, such as Fourier-transform infrared or cavity ring-down spectroscopy (34), are sensitive primarily to H–X stretch overtone states. Dispersed fluorescence (DF) (2, 8, 35) and stimulated

emission pumping (SEP) (2, 19, 20) are based on electronic transitions and therefore give access, through Franck-Condon transitions, to complementary classes of states that involve high excitation in bending and AB stretching vibrations. They are the methods of choice for studying highly excited vibrational states, especially for high bending states.

In principle, DF and SEP spectra yield equivalent information. However, because of the different realizations (spontaneous versus stimulated emission), they complement each other. SEP spectra are typically recorded at resolutions ~100 times higher than DF spectra, but the relative intensity information in a SEP spectrum is usually corrupted by experimental artifacts. The lower resolution of DF spectra is not necessarily a disadvantage, because such spectra contain information exclusively relevant to the early time dynamics of the perfectly specified and initially localized state that is prepared by short-pulse excitation. DF spectra (unresolved features) reveal the most important anharmonic effects, which must be understood first, whereas SEP spectra (eigenstates) sample all anharmonic effects.

Low-resolution DF spectra, originating from different vibrational states in the electronic $\widetilde{C}$ state (36), are depicted in Figure 2. All spectra show a pronounced and long progression in what had been identified as the ν_2 mode, which, in the absence of the theoretical analysis, was believed to reflect bending overtones (37). The bands labeled as *a*–*e* seem not to be members of the even-υ_2 progression. Furthermore, their rotational constants are much larger than those obtained from the analysis of the vibrational levels in the lower-energy region, which indicates that they represent a new family of vibrational states. Because DF spectra are relatively easy to record, they are useful for getting an overview of the vibrational spectrum and dynamics in the ground state.

In a SEP experiment, the output of a tunable dye laser is used to stimulate emission to a particular vibration-rotation state in the electronic ground state. This guarantees ~0.03 cm^{-1} (rotational) spectral resolution. However, only a very narrow energy range (~20 cm^{-1}) can be sampled in a single scan, and in addition, the relative intensities are much more difficult to measure accurately. Figure 3 shows two SEP spectra recorded from the (0, 3, 0) vibrational level in the $\widetilde{C}$ state in the region of the (0, 18, 0) level (36). What was merely one broad line in Figure 2 turns out to consist of transitions into eight different vibrational levels. Actually, what we see here is the (almost) complete [[0, 18]] polyad (see below); for reasons discussed below, the two lowest members of this polyad are not observed because of unfavorable Franck-Condon factors.

Because HCP is linear in the ground electronic state, $\widetilde{X}$, bent excited electronic states are required in order to examine highly excited bending states by DF or SEP spectroscopy. The $\widetilde{A}$ and $\widetilde{C}$ states have significantly bent equilibrium geometries [130° and 113°, respectively (38)]. Because the equilibrium values of the HC bond coordinate in the lower and upper states are similar, only states without excitation in the HC mode, ν_1, are spectroscopically accessible, unless multiple resonance or hot-band excitation schemes are used. That is why the spectra in Figures 2 and 3 are relatively sparse. Lehmann et al (37) were the first to study highly excited

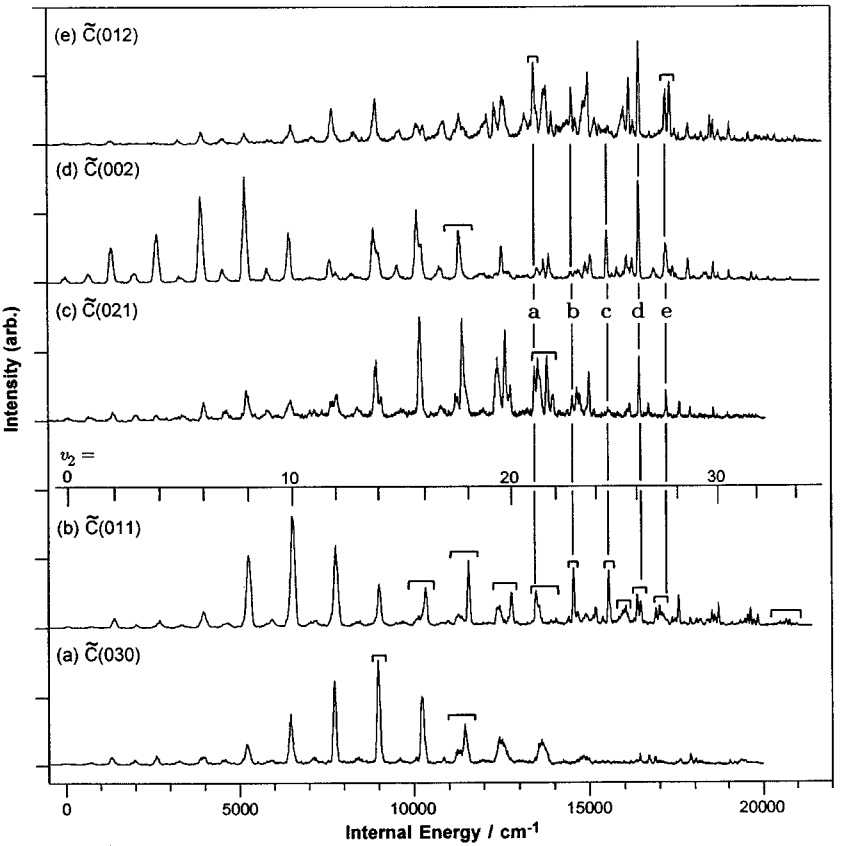

Figure 2 Dispersed fluorescence spectra of the $\widetilde{C} \rightarrow \widetilde{X}$ transition of HCP. The intermediate levels used are indicated. (*Horizontal bars*) Vibrational bands that are investigated by stimulated emission pumping spectroscopy. (From Reference 36; reprinted with the permission of the American Institute of Physics.)

vibrational levels in the ground state of HCP. They recorded and analyzed (high-resolution) $\widetilde{A} - \widetilde{X}$ DF spectra and observed 94 vibrational levels, all of which were assigned to pure overtones and combinations of the v_2 and the CP stretch v_3 modes. The highest overtone reported was $v_2 = 27$, corresponding to an energy (above the zero-point level) of 16,912 cm^{-1}. Despite the high excitation in the bending mode, v_2, a surprisingly regular harmonic-like behavior was observed; no features in the spectrum that might be attributed to isomerization were found.

The initial survey of Lehmann et al was later extended by Chen et al (39) and Ishikawa et al (40), who primarily sampled the pure $(0, v_2, 0)$ overtones from $v_2 = 26$ through 42, thereby probing a much higher energy regime. They recorded SEP spectra via the $\widetilde{A} - \widetilde{X}$ and $\widetilde{C} - \widetilde{X}$ transitions. Later, Ishikawa et al (36)

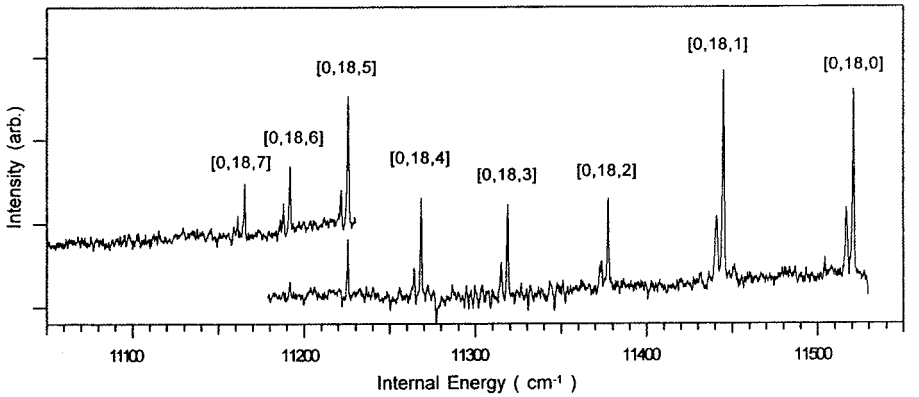

Figure 3 Stimulated emission pumping spectrum of HCP in the region of the [[0, 18]] polyad. The nomenclature [0, 18, $0 \leq i \leq 9$] indicates the HC stretch quantum number, the polyad quantum number, and the position inside the polyad, respectively. The *low-intensity lines* next to the *main lines* represent a different rotational transition. (From Reference 36; reprinted with the permission of the American Institute of Physics.)

extended the SEP measurements to the lower-energy regime and analyzed many combination levels $(0, v_2, v_3)$ of the [[0, 14]]–[[0, 34]] polyads.

The two crucial observations emerging from the SEP studies were a sudden onset of perturbations at $v_2 \geq 32$ and the onset of rapid changes of all of the vibrational fine-structure constants in the vicinity of $v_2 = 36$. For example, the rotational constant increases by about 8% from $v_2 = 34$ to 42. It was surmised that these drastic changes are consequences of a qualitative change of the potential along the isomerization path as HC bonding gradually changes into predominantly HP bonding, resulting in a significant change of the H–CP stretching frequency. Thus, both the onset of perturbations and the abrupt changes of the molecular vibration-rotation fine-structure constants were suggested as diagnostic of the onset of isomerization.

However, the "story" encoded in the vibration-rotation spectrum is more complicated. Large rotational constants are indeed a fingerprint of the motion along the isomerization path—but in a different way than was originally proposed by Ishikawa et al (40). Because of the incompleteness of the experimental spectra and because of the fact that without examining the nodal structure of the quantum mechanical wave functions unique assignments are almost impossible at high energies.

POTENTIAL ENERGY SURFACE

An accurate global PES is the cornerstone for the quantum mechanical calculation of vibrational energies. "Global" means here that the PES covers a large part of the energetically accessible coordinate space rather than only the region around the equilibrium geometry. For HCP, the surface must extend all the way from the

linear HCP equilibrium structure to the CPH saddle point; in addition, the CP and HC bond distances must be varied over large ranges. In previous studies we employed a global ab initio potential (41, 42). However, although this earlier version did describe some of the peculiar aspects of the vibrational dynamics of HCP in a qualitatively correct manner, it was not sufficiently accurate to allow direct comparisons between calculated and observed vibrational energy levels. Two other, very accurate PESs had only been constructed in regions near the linear potential minimum and were thus not suitable for calculating the spectrum at high excitation energies, where large-amplitude bending motion is important (43–45).

To make direct contact with experiment, we constructed a completely new PES that covers a wide range of nuclear geometries. About 1100 points on the PES have been calculated at a high level of ab initio theory (multireference configuration interaction with a large atomic basis set). The calculated points are subsequently fitted to a complex analytical expression that was then used to compute the vibrational energy levels (46). Fitting a global PES, which covers a wide range of coordinates far from equilibrium and a wide range of energies, more than 25,000 cm^{-1} in the present case, with an accuracy of about 10–20 cm^{-1}, is not an everyday task—even if only three vibrational degrees of freedom are involved. A power series expansion of the PES is certainly not appropriate; the global potential fit includes, in some sense, all powers of coordinate displacements.

The transition frequencies for the three vibrational fundamentals, as obtained from the fitted PES, are 3216.2 (3216.889) cm^{-1}, 1332.3 (1334.980) cm^{-1}, and 1262.5 (1278.278) cm^{-1} for states (1, 0, 0), (0, 2, 0), and (0, 0, 1), respectively [the numbers in parentheses are from the high-resolution Fourier-transform infrared data of Jung et al (47)]. Although the values for the HC stretching mode (ν_1) and mode ν_2 agree well with their experimental counterparts, the frequency of the CP stretching mode (ν_3) is underestimated by 16 cm^{-1}. A deviation as small as 16 cm^{-1} for only one vibrational mode is quite good for an ab initio calculation. However, if the molecule is excited by many vibrational quanta, the error quickly accumulates to a value that prohibits making unique correspondences between calculated and observed energy levels. Therefore, we applied a simple scaling correction to the CP coordinate, including only a single parameter. This parameter was not adjusted to minimize the error for the fundamental, rather it was chosen so that good overall agreement over a large energy region is obtained. The fundamental frequencies for the improved potential are 3216.6 cm^{-1}, 1333.7 cm^{-1}, and 1274.6 cm^{-1}, in good agreement with the experimental values. An indication of how well the quantum mechanical calculation reproduces the measured spectrum up to high energies is given below.

Figure 4 shows a contour plot of the HCP PES for a fixed CP bond distance. (In what follows, potential energies are measured with respect to the energy at the HCP equilibrium geometry.) There is only one stable minimum, H–CP; the linear CP–H configuration is a saddle point on the three-dimensional PES (see also 37, 42). Therefore, it is, strictly speaking, not justified to allude to isomerization in HCP. However, the large-amplitude bending motion, on which we focus in this article,

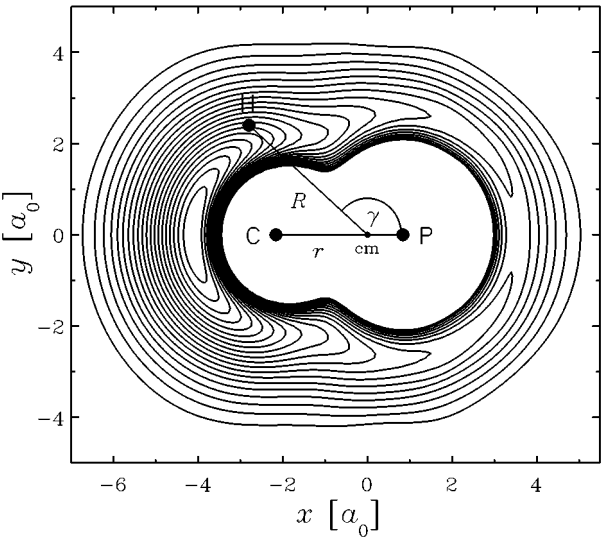

Figure 4 Contour plot of the HCP ground-state potential energy surface. The energy for the lowest contour is 0.236 eV and the spacing is 0.25 eV. Energies are relative to $E = 0$ at the HCP minimum. The CP bond distance is fixed at $r = 2.893\,a_0$. cm, center-of-mass of CP; R, r, and γ, the Jacobi coordinates described in the text.

can be viewed as a precursor of isomerization. The contour plot intriguingly reflects the quite different "radii" of the carbon and phosphorous atoms, which lead to the pronounced "waist" of the peanut-like structure. The corresponding minimum-energy path from H–CP to CP–H, depicted in Figure 5, reveals a drastic slope change exactly in this waist region between $120^\circ \lesssim \gamma \lesssim 130^\circ$. Although $V(\gamma)$ is harmonic in the H–CP hemisphere, it becomes surprisingly anharmonic in the CP–H hemisphere. The slight undulations between 50° and 90° are partly due to the analytical fit (46). It is the narrow angular region of the waist, which was difficult to fit, that causes the profound structural changes in the energy spectrum and the wave functions that we highlight below.

FULL QUANTUM MECHANICAL APPROACH

Once the PES is known, the vibrational-rotational eigenvalue spectrum of a triatomic molecule can be calculated exactly by solving the Schrödinger equation

$$(\hat{H} - E)\Psi = 0, \qquad 1.$$

where $\hat{H}$ is the Hamiltonian operator and Ψ is the total wave function of the molecular system. In the current calculations we use Jacobi coordinates, **R** and **r**, to describe the internal motion of the molecule (48); **R** is the vector from H to

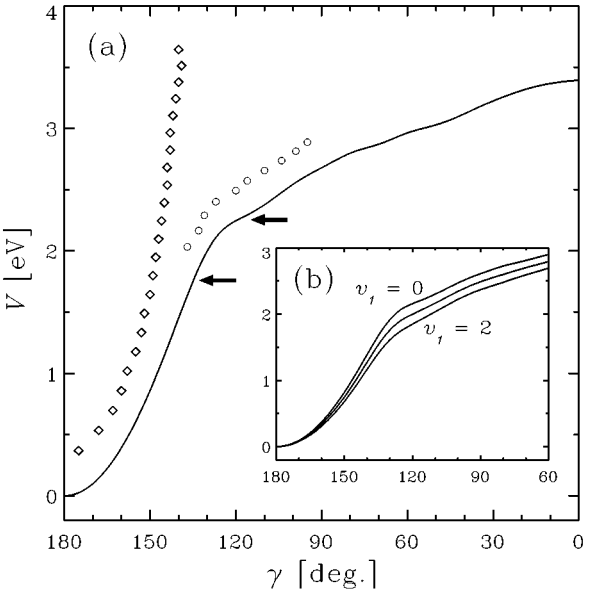

Figure 5 (*a*) Potential energy as a function of the Jacobi angle γ along the minimum-energy path; the potential is minimized in the two stretch coordinates R and r. (*Diamonds*) Outer maxima of the eigenfunctions of states $(0, v_2, 0)$; (*circles*) outer maxima of the eigenfunctions of states $(0, v_2, 0)_I$; (*arrows*) first two saddle-node bifurcations of the classical phase space. (*b*) Cuts along the minimum-energy paths of the two-dimensional adiabatic potentials $\widetilde{V}_{v_1}(r, \gamma)$ for HC stretching quantum numbers $v_1 = 0$, 1, and 2. For comparison, all *curves* are vertically shifted to have the same minimum value at the linear HCP geometry. See the text for more details.

the center-of-mass of CP and **r** is the vector joining the atoms C and P (Figure 4). Depending on the particular molecule (two energetically accessible dissociation channels, two equivalent bond coordinates, etc), other coordinate systems such as hyperspherical, Radau, or valence coordinates might be more appropriate (49). Nevertheless, all these coordinate systems allow numerically exact solutions of the Schrödinger equation (7, 50). Various types of two-dimensional contour plots of the HCP PES in Jacobi coordinates are depicted in Figure 6, together with selected wave functions and classical periodic orbits.

After making the transformation $\Psi(\mathbf{R}, \mathbf{r}) \rightarrow Rr\Psi(\mathbf{R}, \mathbf{r})$, the Hamiltonian operator is given by (48)

$$\hat{H} = -\frac{\hbar^2}{2\mu_R}\frac{\partial^2}{\partial R^2} + \frac{1}{2\mu_R R^2}\hat{l}^2 - \frac{\hbar^2}{2\mu_r}\frac{\partial^2}{\partial r^2} + \frac{1}{2\mu_r r^2}\hat{j}^2 + V(R, r, \gamma), \qquad 2.$$

where μ_R and μ_r are the reduced masses for H–CP and CP, respectively, and γ is the angle between the two vectors **R** and **r**. $\hat{l}$ is the orbital angular momentum

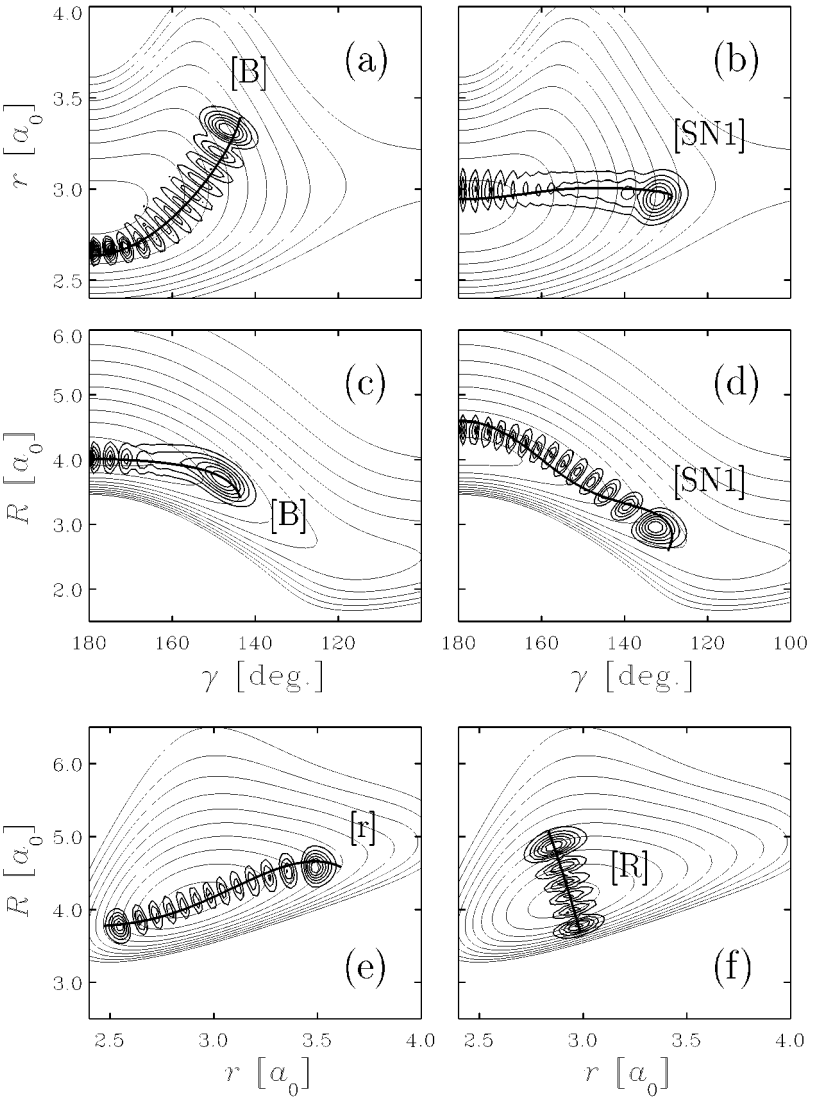

Figure 6 Two-dimensional contour plots of the HCP potential energy surface in Jacobi coordinates R, r, and γ. The energy of the lowest contour is 0.236 eV and the contour spacing is $\Delta E = 0.5$ eV. Also shown are examples of quantum mechanical wave functions ($\sin\gamma|\Psi|^2$) and the corresponding classical periodic orbits. The assignments of the states are (*a*, *c*) (0, 24, 0); (*b*, *d*) $(0, 26, 0)_{\mathrm{I}}$; (*e*) (0, 0, 12); and (*f*) (5, 0, 0). The energies of the quantum levels and the classical orbits roughly correspond to each other. See the text for further details.

operator associated with **R**, and $\hat{j}$ is the rotational angular momentum related to **r**. To account for the conservation of the total angular momentum $\hat{J}$, one can replace $\hat{j}^2$ by $(\hat{J}+\hat{l})^2$ and obtain, after some straightforward algebra (51, 52),

$$\hat{H} = -\frac{\hbar^2}{2\mu_R}\frac{\partial^2}{\partial R^2} - \frac{\hbar^2}{2\mu_r}\frac{\partial^2}{\partial r^2} + \frac{1}{2\mu_R R^2}\hat{l}^2 + \frac{1}{2\mu_r r^2}(\hat{J}^2 + \hat{l}^2 - 2\hat{J}_z\hat{l}_z)$$
$$+ V(R, r, \gamma) - \frac{1}{2\mu_r r^2}(\hat{J}_+\hat{l}_- + \hat{J}_-\hat{l}_+), \qquad 3.$$

where the index z denotes components of the angular momenta with respect to the projection on the molecule-fixed z-axis, the CP bond in the present case, and the indices $\pm$ indicate the appropriate raising and lowering operators (the raising/lowering roles of $J_\pm$ are reversed here). The last term in Equation 3 (Coriolis coupling) is responsible for the coupling between states with different K quantum numbers, where K is the body-fixed z-axis projection quantum number for both $\hat{J}$ and $\hat{l}$. K corresponds to the vibrational angular momentum of a linear molecule (which is conventionally labeled l). It is, in principle, not a conserved quantum number; however, if the coupling between different K-states is small, one can consider K to be a good quantum number.

Alternative schemes to construct appropriate basis sets to expand the wave function $\Psi(\mathbf{R}, \mathbf{r})$ and to represent the Hamiltonian are described in the literature (53, 54, 54a). One usually starts with products of one-dimensional basis functions, i.e. spherical harmonics for the angle γ and oscillator wave functions for the two stretch coordinates R and r. In order to represent highly excited states, a very large number of such "primitive" basis functions are required (several hundred thousand). The resulting Hamiltonian matrix can be diagonalized by an iterative procedure (55–57). However, the matrix dimension is generally too large for direct diagonalization. By applying various contraction/truncation schemes (49, 58), the dimension can be reduced to manageable size ($N < 10{,}000$ or so). Direct diagonalization has the advantage that all relevant eigenvalues and eigenstates are obtained at once. However, because of the limited size of the basis set, the accuracy generally decreases with increasing energy. Nevertheless, direct diagonalization is the method we applied in the current study; more details about the numerical procedure are given elsewhere (46, 59), and some indications concerning the accuracy of the variational calculations are given below, where the results are discussed. An alternative and very efficient approach is provided by "filter diagonalization" (60, 61).

Calculations for total angular momentum $J \geq 1$, required for extracting rotational constants, are considerably more demanding because, as a result of Coriolis interaction, the basis size increases by a factor of J or $J+1$, depending on the parity (48). The problem is overcome by first performing approximate calculations for fixed values of the projection quantum number K, ignoring the Coriolis coupling, i.e. the last term in Equation 3. The resulting approximate wave functions for fixed K are used in a second step as basis functions for the exact Hamiltonian, inclusive of the Coriolis interaction term (52, 59, 62).

Whatever method is used for solving the eigenvalue problem, the asset of the quantum mechanical calculations is that they provide the wave functions as functions of all three internal coordinates. Wave function plots are essential for unique assignments of states and to understand the story encoded in the vibration-rotation spectrum. A few examples of uniquely assignable wave functions are presented in Figure 6. Figure 7 depicts wave function plots for all eigenstates belonging to one particular polyad, [[0, 14]]. The R-axis is perpendicular to the (r, γ)-plane and not seen here. The actual assignments are discussed in the next section. For $J = K = 0$, the wave functions are symmetric with respect to the linear geometry and, therefore, only even values of v_2 are possible. States with odd values of v_2 occur for $K = 1, 3, \ldots$. The wave functions for $K > 0$ have a node at linearity. Any kind of automatic assignment, for example, by means of the expectation values of the kinetic energy operators corresponding to R, r, and γ, would be helpful

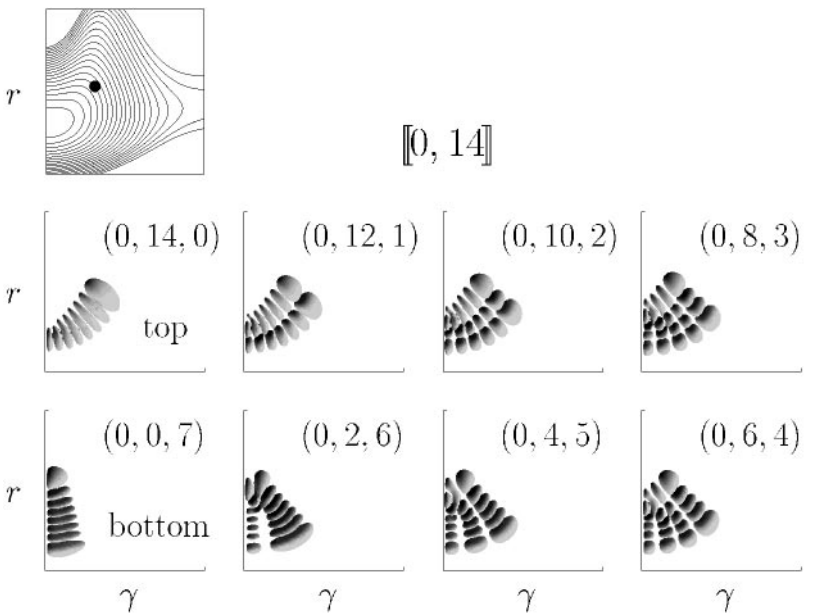

Figure 7 Wave functions for the complete polyad [[0, 14]]. The *horizontal axis* ranges from $\gamma = 180^\circ$ to 100°; the *vertical axis* ranges from $r = 2.40$ a_0 to 4.00 a_0. Plotted is one particular contour of the function $\sin\gamma\,|\Psi(R, r, \gamma)|^2$. The plots are viewed along the R-axis, i.e. in a direction perpendicular to the (r, γ)-plane. Because of the $\sin\gamma$ weighting factor, there is a node at the linear configuration irrespective of whether v_2 is even or odd. In order to illustrate how the wave functions are nested in the well of the potential energy surface, a two-dimensional contour plot for fixed value of R is also shown. The *heavy dot* marks the equilibrium geometry in the $\widetilde{A}$ state. The energy decreases from state (0, 14, 0) to state (0, 0, 7).

but is not sufficient at higher energies, when unexpected structures develop. In the case of HCP, the first thousand eigenfunctions have been visually inspected, one state after the other (59, 63). Only by such a careful systematic procedure can the big picture be revealed.

The tabulated results of the quantum mechanical calculations (energies, assignments, rotational constants, etc) are available (R Schinke, personal communication). In general, the agreement with the measured energies is very gratifying. Of course, comparison can only be made with those states that can be unambiguously assigned in the experimental spectrum. However, most of the experimentally observed levels are assigned. There are some unassigned states, for which clear-cut comparisons with calculated states seem hopeless (see for example 40:Table 9). The results for four polyads, discussed below, exemplify the degree of agreement between theory and experiment [see Table 1 (online only; also available through http://AnnualReviews.org, Electronic Materials)]. The accuracy of the variational calculations is estimated to be of the order of 0.1 cm^{-1} for the highest of these four polyads.

POLYADS

Polyad Structure and Wave Functions

The principal feature of the energy-level spectrum of HCP is a pronounced 2:1 anharmonic resonance between modes 2 and 3, i.e. $2\nu_2 \approx \nu_3$ (1335 $cm^{-1} \approx$ 1278 cm^{-1}). This resonance leads to a well-defined clustering of the vibrational spectrum in terms of polyad $[[v_1, P]]$ with polyad quantum number $P = v_2 + 2v_3 = 0, 1, 2, \ldots$; in this article, only polyads with even values of P are discussed. The polyad pattern was crucial to the initial assignments of the experimental spectra at high vibrational energy (36, 40). All states having the same P (and HC stretch quantum number v_1) have approximately the same energy. There are $(P + 2)/2$ and $(P + 1)/2$ individual states in each polyad for even and odd values of P, respectively. Their assignments are $(v_1, P - 2v_3, v_3)$; alternatively, we occasionally use the notation $[v_1, P, i]$, with i indicating the position within the polyad ($i = 0$ for the top state) (see Figure 3). In Figure 8 we illustrate the energy-level structure in the region of the [[0, 8]]–[[0, 16]] polyads. For a given value of v_1, a relatively large energy gap separates adjacent polyads, at least in this lower-energy regime. For the discussion below, note that another resonance may have an important effect on the level structures and dynamics: One quantum of the ν_1 mode is worth roughly five quanta of the ν_2 mode, i.e. the states belonging to polyads $[[0, P]]$ have roughly the same energies as the states in polyads $[[1, P-5]]$ and $[[2, P-10]]$, etc. Because ν_1 changes slightly with P, the precise locations of the $[[1, P-5]]$ and the $[[2, P-10]]$ polyads with respect to $[[0, P]]$ also change with excitation energy.

The systematic evolution of the nodal patterns of the wave functions within a polyad is illustrated in Figure 7 for polyad [[0, 14]]. Highlighted is the (r, γ)

TABLE 1 Comparison of calculated (QM), fitted (fit A and fit B), and measured (Exp.) vibrational energies (in cm^{-1}, relative to the ground vibrational state) for four selected polyads (experimental data from Reference 36: Table 2)

no.[a]	$[v_1, P, i]$[b]	(v_1, v_2, v_3)	QM	Fit A[c]	Fit B[d]	Exp.
22	[0,10,5]	(0,0,5)	6298.42	1.6	6274.4	—
24	[0,10,4]	(0,2,4)	6334.42	−3.9	6331.9	6328.0
25	[0,10,3]	(0,4,3)	6369.65	1.7	6364.2	6367.0
26	[0,10,2]	(0,6,2)	6411.63	2.4	6406.5	6411.0
27	[0,10,1]	(0,8,1)	6459.21	0.4	6458.3	6464.0
28	[0,10,0]	(0,10,0)	6515.70	−0.8	6518.9	6522.0
87	[0,18,9]	(0,0,9)	11121.48	−0.6	11078.6	—
88	[0,18,8]	(0,2,8)	11158.53	4.8	11150.0	—
89	[0,18,7]	(0,4,7)	11175.09	0.9	11157.5	11161.2
90	[0,18,6]	(0,6,6)	11200.19	2.9	11189.2	11187.8
92	[0,18,5]	(0,8,5)	11233.99	3.2	11222.2	11221.4
93	[0,18,4]	(0,10,4)	11273.71	2.2	11264.6	11264.1
95	[0,18,3]	(0,12,3)	11319.64	0.0	11315.0	11314.9
98	[0,18,2]	(0,14,2)	11374.31	−1.4	11373.6	11373.4
100	[0,18,1]	(0,16,1)	11440.87	−0.3	11441.1	11440.7
101	[0,18,0]	(0,18,0)	11521.58	3.4	11518.7	11516.7
145	[0,22,11]	$(0,22,0)_I$	13429.86	−12.1	13403.1	13426.9
147	[0,22,10]	(0,0,11)	13457.28	−3.9	13435.2	—
148	[0,22,9]	$(0,20,1)_I$	13503.55	−3.6	13495.0	—
149	[0,22,8]	((0,6,8))[e]	13519.99	−3.2	13502.3	—
150	[0,22,7]	(0,8,7)	13548.88	0.5	13538.9	13534.9
152	[0,22,6]	(0,10,6)	13580.56	0.6	13567.9	13566.5
153	[0,22,5]	(0,12,5)	13620.50	1.0	13609.3	13607.8
155	[0,22,4]	(0,14,4)	13666.06	−0.3	13658.5	13657.4
157	[0,22,3]	(0,16,3)	13719.37	−1.9	13716.0	13715.5
159	[0,22,2]	(0,18,2)	13783.51	−1.8	13782.4	13782.0
162	[0,22,1]	(0,20,1)	13859.73	−0.9	13858.6	13857.5
164	[0,22,0]	(0,22,0)	13947.86	−1.9	13946.1	13942.0
286	[0,30,15]	$(0,30,0)_I$	17128.58	−15.5	17181.7	17172.4
307	[0,30,14]	$(0,28,1)_I$	17534.52	−4.4	17544.4	—
319	[0,30,13]	$(0,26,2)_I$	17831.55	12.5	17804.3	—
328	[0,30,12]	(0,0,15)	17997.00	7.7	17888.1	—

(*continued*)

TABLE 1 (*continued*)

no.[a]	[v_1, P, i][b]	(v_1, v_2, v_3)	QM	Fit A[c]	Fit B[d]	Exp.
329	[0,30,11]	$(0,24,3)_I$	18001.40	−1.2	17979.2	—
332	[0,30,10]	(0,2,14)	18067.58	−3.9	18013.0	—
335	[0,30,9]	$(0,22,4)_I$	18106.74	5.1	18084.2	—
337	[0,30,8]	((0,14,8))[d]	18124.2	1.3	18097.4	—
338	[0,30,7]	(0,16,7)	18157.95	2.4	18137.6	—
341	[0,30,6]	(0,18,6)	18195.42	−0.5	18177.8	—
343	[0,30,5]	((0,20,5))[d]	18241.11	−3.8	18230.2	—
346	[0,30,4]	(0,22,4)	18302.02	−0.6	18292.1	18292.4
348	[0,30,3]	(0,24,3)	18370.28	0.0	18363.8	18366.6
355	[0,30,2]	((0,26,2))[d]	18453.18	3.3	18446.0	18448.9
361	[0,30,1]	(0,28,1)	18549.23	5.3	18534.0	18536.7
366	[0,30,0]	(0,30,0)	18656.61	1.6	18647.0	18648.0

[a]Number of calculated bound state.

[b]v_1, HC stretch quantum number; $P = v_2 + 2v_3$, polyad quantum number; i, position inside the polyad, $i = 0$ for the highest level.

[c]Energies obtained from the fit of the full quantum mechanical spectrum; listed are the deviations from the original values.

[d]Energies obtained from the fit of the experimental spectrum.

[e]Double brackets indicate states that are not pure, i.e. states that show a high degree of mixing with a nearby state.

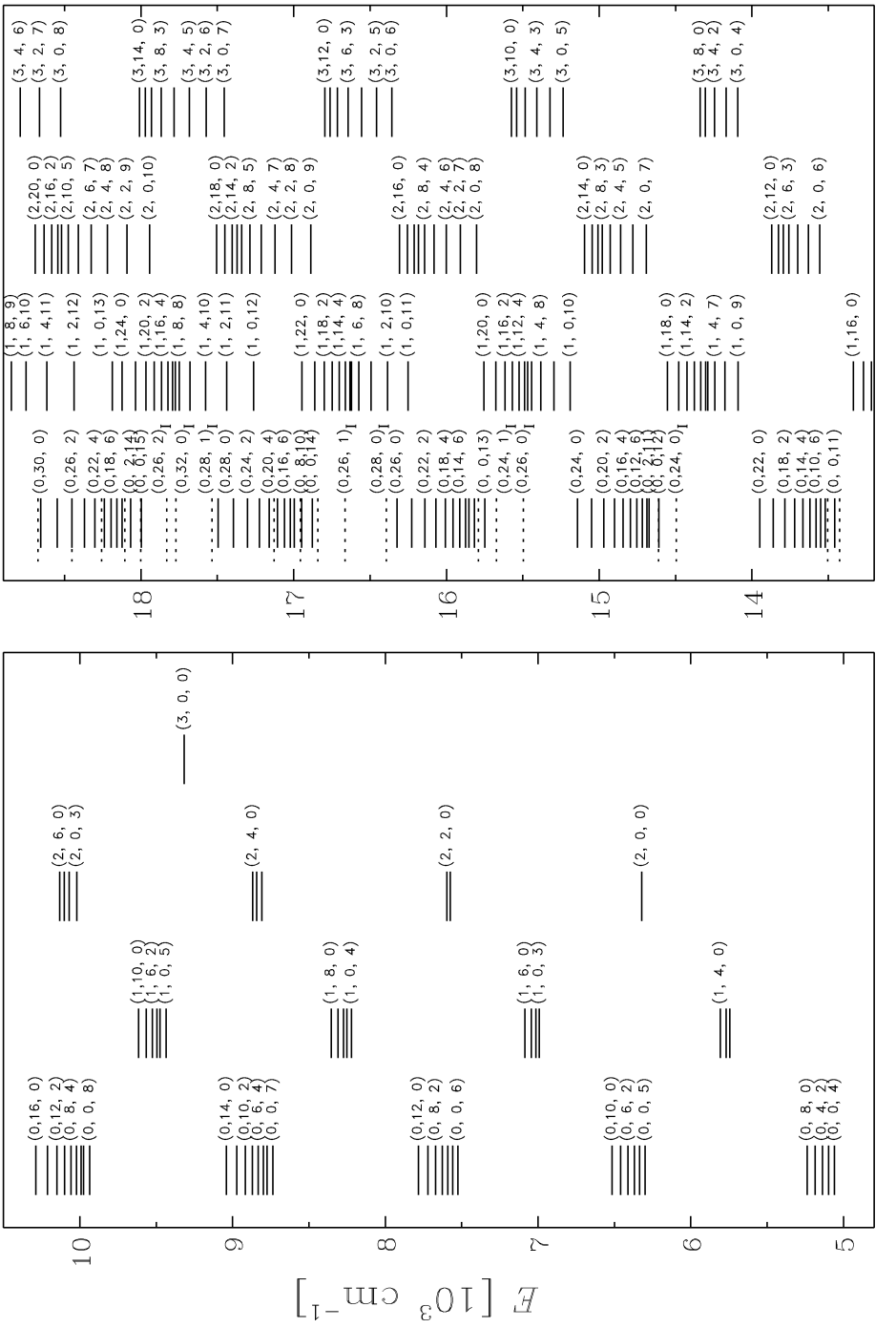
E [10³ cm⁻¹]
5
6
7
8
9
10
14
15
16
17
18
(0,16, 0)
(0,12, 2)
(0, 8, 4)
(0, 0, 8)
(0,14, 0)
(0,10, 2)
(0, 6, 4)
(0, 0, 7)
(0,12, 0)
(0, 8, 2)
(0, 0, 6)
(0,10, 0)
(0, 6, 2)
(0, 0, 5)
(0, 8, 0)
(0, 4, 2)
(0, 0, 4)
(1,10, 0)
(1, 6, 2)
(1, 0, 5)
(1, 8, 0)
(1, 0, 4)
(1, 6, 0)
(1, 0, 3)
(1, 4, 0)
(2, 6, 0)
(2, 0, 3)
(2, 4, 0)
(2, 2, 0)
(2, 0, 0)
(3, 0, 0)
(0,30, 0)
(0,26, 2)
(0,22, 4)
(0,18, 6)
(0,32, 0)
(0,28, 1)
(0,28, 0)
(0,24, 2)
(0,20, 4)
(0,16, 6)
(0,26, 1)
(0,28, 0)
(0,26, 0)
(0,22, 2)
(0,18, 4)
(0,14, 6)
(0, 0,13)
(0,24, 1)
(0,26, 0)
(0,24, 0)
(0,20, 2)
(0,16, 4)
(0,12, 6)
(0, 8,11)
(0, 0,12)
(0,24, 0)
(0,22, 0)
(0,18, 2)
(0,14, 4)
(0,10, 6)
(0, 0,11)
(1, 8, 9)
(1, 6,10)
(1, 4,11)
(1, 2,12)
(1, 0,13)
(1,24, 0)
(1,20, 2)
(1,16, 4)
(1, 8, 8)
(1, 4,10)
(1, 2,11)
(1, 0,12)
(1,22, 0)
(1,18, 2)
(1,14, 4)
(1, 6, 8)
(1, 2,10)
(1, 0,11)
(1,20, 0)
(1,16, 2)
(1,12, 4)
(1, 4, 8)
(1, 0,10)
(1,18, 0)
(1,14, 2)
(1, 4, 7)
(1, 0, 9)
(1,16, 0)
(2,20, 0)
(2,16, 2)
(2,10, 5)
(2, 6, 7)
(2, 4, 8)
(2, 2, 9)
(2, 0,10)
(2,18, 0)
(2,14, 2)
(2, 8, 5)
(2, 4, 7)
(2, 2, 8)
(2, 0, 9)
(2,16, 0)
(2, 8, 4)
(2, 4, 6)
(2, 2, 7)
(2, 0, 8)
(2,14, 0)
(2, 8, 3)
(2, 4, 5)
(2, 0, 7)
(2,12, 0)
(2, 6, 3)
(2, 0, 6)
(3, 4, 6)
(3, 2, 7)
(3, 0, 8)
(3,14, 0)
(3, 8, 3)
(3, 4, 5)
(3, 2, 6)
(3, 0, 7)
(3,12, 0)
(3, 6, 3)
(3, 2, 5)
(3, 0, 6)
(3,10, 0)
(3, 4, 3)
(3, 0, 5)
(3, 8, 0)
(3, 4, 2)
(3, 0, 4)

dependence of the wave functions, which, because of the $2\nu_2 \approx \nu_3$ resonance, is more interesting than the behavior with respect to R; for $v_1 = 0$, all wave functions have a Gaussian-type shape along the R axis, the axis perpendicular to the (r, γ)-plane. In the case of the pure $(0, v_2, 0)$ overtones, v_2 specifies the number of nodes along the backbone of the wave function from $\gamma = 0^\circ$ all the way to 360°, as is customary for a molecule with linear equilibrium geometry. The pure $(0, 0, v_3)$ states have v_3 nodes along their backbones. They are essentially aligned along the axis of the CP stretch coordinate r, i.e. the $(0, 0, v_3)$ overtones are almost pure CP stretching states. For all polyads up to [[0, 20]], the pure v_2 overtones $(0, v_2, 0)$ lie at the top of the polyad, whereas the pure v_3 overtones $(0, 0, v_3)$ are located at the bottom. Between these energetic extremes within each polyad, the wave functions are easily recognized as $(0, P-2, 1)$, $(0, P-4, 2)$, etc. All polyads $[[0, P \leq 14]]$ have the same general behavior. However, with [[0, 16]], some slight changes appear at the bottom of the polyads that become fully developed by $P = 22$.

Pure v_2- and v_3-Overtones

The pure v_2-progression has received the most experimental attention. The lowest members have been precisely measured by microwave and infrared spectroscopy (47), and the states up to $v_2 \leq 27$ have been studied by DF (37). Ishikawa et al (40) observed the overtones $v_2 = 26-42$ by SEP and extracted for all states the vibrational fine-structure constants, which, as shown below, contain valuable information about the dynamics of these vibrational levels.

The $(0, v_2, 0)$ states are very robust, which means they form regular series that are easily recognizable up to very high energies, where many other states are unassignable because of complex mixings among neighboring (zero-order) states. The wave functions of the $(0, v_2, 0)$ states do not change their general shape, except for accidental admixtures from near-degenerate states; with increasing energy, successively more "pearls" are added to the "necklace." The energy spacing between adjacent $(0, P, 0)$ states as a function of P (Figure 9*a*) is essentially a straight line, which indicates that the transition energies can be well represented by a (Morse-like) power series in v_2 up to second order.

The calculated transition energies for the pure v_2 overtones can be compared with experimental data up to $v_2 = 42$. The deviation $E_{\text{th.}} - E_{\text{ex.}}$ is negative from $v_2 = 2-14$, becomes positive at $v_2 = 16$, and then monotonically increases up to $v_2 = 42$. The root mean square deviation for states $(0, 2, 0) - (0, 32, 0)$ is only 6.6 cm^{-1}, but it increases to 16 cm^{-1} when all states up to $v_2 = 42$ are included. The deviation is 10.2 cm^{-1} for $v_2 = 32$ and rises to 41 cm^{-1} for $v_2 = 42$. The estimated error due to the limited basis set in the variational calculations is 0.3 cm^{-1} for $v_2 = 32$ and 0.5 cm^{-1} for $v_2 = 42$.

←

Figure 8 Energy-level spectrum in the regions of (*left*) polyads [[0, 8]]–[[0, 16]] and (*right*) polyads [[0, 22]]–[[0, 30]]. (*Dotted lines*) The isomerization eigenstates $(v_1, v_2, v_3)_{\text{I}}$. Energy is normalized with respect to $E = 0$ at the (0, 0, 0) level.

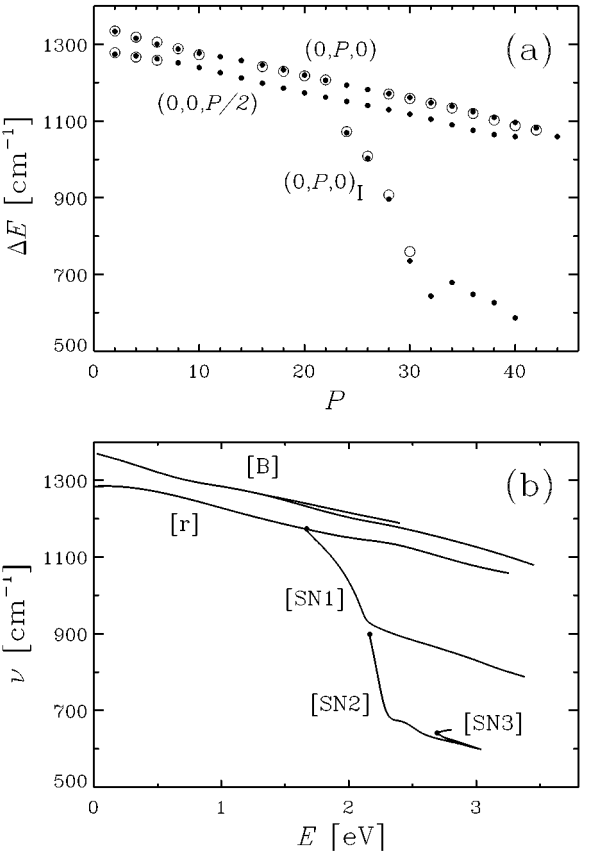

Figure 9 (*a*) Energy differences [$\Delta E = E_{(0,P,0)} - E_{(0,P-2,0)}$, etc] between neighboring states of the progressions $(0, P, 0)$, $(0, 0, P/2)$, and $(0, P, 0)_I$ versus polyad quantum number P. (*Black dots*) Quantum mechanical results; (*open circles*) experimentally observed energy levels. (*b*) The frequencies of the various families of periodic orbits as functions of energy (relative to $E = 0$ at the bottom of the potential well). (*Dots*) Saddle-node bifurcations, discussed in the text. The *horizontal axes* in (*a*) and (*b*) roughly correspond to each other.

One extremely important point must be made here: The $(0, v_2, 0)$ wave functions start out as true bending wave functions at the bottom of the energy-level spectrum, i.e. their backbones are predominantly aligned along the angular (bending) axis. Thus, as the energy in this mode is increased, one naturally expects the corresponding wave functions to monotonically follow the isomerization path all the way from the H–CP side to the CP–H hemisphere. However, that is not what happens. With increasing energy, the v_2 overtones evolve toward larger and larger CP bond distances r, i.e. they acquire more and more CP stretch character (see

Figure 7). Contrary to expectation, the $(0, v_2, 0)$ wave functions are confined to a small angular range around linearity. This is illustrated in Figure 5*a*, where the angle γ_{max} at which the wave functions have maximal amplitude is plotted versus energy; γ_{max} is the quantum mechanical counterpart of the angle at the classical turning point. Even for the highest states considered, the maximal bending amplitude around linearity is restricted to merely $\pm 40^\circ$. Thus, even when the energies of the high-v_2 states lie well above the energy where the minimum-energy-path potential departs from the diabatic part by leveling off to the CP–H side, the $(0, v_2, 0)$ wave functions do not follow this adiabatic path.

The pure $(0, 0, v_3)$ states are also robust and may easily be followed to very high energies. As the quantum number v_3 increases, they align themselves more and more along the r-axis, i.e. they behave more and more like pure CP stretching states. Because of unfavorable Franck-Condon factors—the $(0, 0, v_3)$ states are centered around $\gamma = 180^\circ$ whereas the $\widetilde{A}$ and $\widetilde{C}$ states are strongly bent—only states up to $v_3 = 3$ have been observed experimentally (37). In particular, that is why the lowest two states of the [[0, 18]] polyad are missing in the SEP spectrum in Figure 3. The root mean square deviation of our calculated values from the measured ones is 2.8 cm^{-1}. The energy spacing between adjacent levels of the v_3 progression is also a linear function and parallels the curve for the $(0, P, 0)$ states up to high quantum numbers (Figure 9).

Genesis of Isomerization States

Wave functions that follow the minimum-energy isomerization path exist—but they only appear at higher energies. The reasons they suddenly are born at relatively high energies, and how their abrupt emergence causes the polyad structure to change, provide deep insight into how a vibrational energy spectrum, which behaves in a "normal" and predictable manner at low energies, changes with energy.

The qualitative mutation of the wave functions first appears in the lower-energy parts of the polyads, whereas the wave functions near the top change gradually and in a predictable manner. To illustrate the structural changes, we show in Figure 10 the four lowest energy wave functions in polyads [[0, 16]]–[[0, 22]]. Beginning with $P = 18$, the wave function of the second-to-lowest state, (0, 2, 8), gradually changes its shape in the (r, γ)-plane, namely it behaves more like what is expected for a real bending state. Subtle signs of this metamorphosis appear in the lower polyads (see $P = 16$) but become incontrovertible for $P = 18$ and 20. The assignments (0, 2, 8) and (0, 2, 9) here reflect more the positions of these states within their respective polyads than the character of the wave function. The mutation of the $(0, 2, P/2 - 1)$ states continues with increasing energy, and more and more states in the lower-energy part of each polyad become participants in this process. Because the new form of the bending states follows the isomerization path, we assign these states as $(v_1, P, 0)_I$, $(v_1, P - 2, 1)_I$, etc, where the subscript I stands for isomerization. The isomerization states are the real bending states.

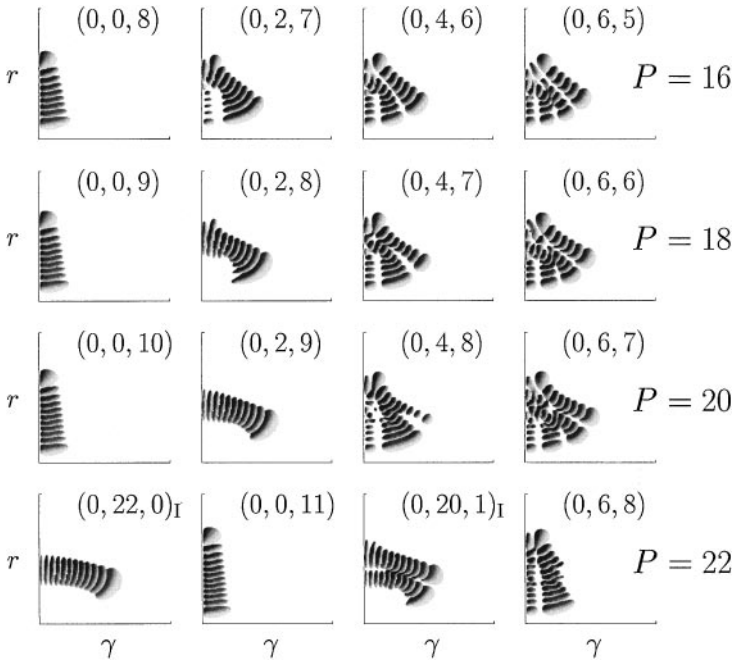

Figure 10 Illustration of the genesis of isomerization states. The wave functions shown are for the lowest four eigenstates of polyads [[0, 16]]–[[0, 22]]. The axes have the same ranges as in Figure 7. Within each row the states are in order of increasing energy (*left to right*).

The potential substantially levels off along the minimum-energy path, toward the CP–H hemisphere (see Figure 5), and as a consequence, the $(0, P, 0)_{\mathrm{I}}$ progression is considerably more anharmonic than is the pure v_2-progression; the gap between neighboring $(0, v_2, 0)_{\mathrm{I}}$ energy levels drops rapidly with increasing value of P (Figure 9). The result is that the energies of the $(0, P, 0)_{\mathrm{I}}$ states fall rapidly relative to the corresponding $(0, 0, P/2)$ states, as seen in Figure 10 for $P = 22$ as well as in Figure 8. It should be emphasized that—in view of the number of nodes—the states $(0, 22, 0)_{\mathrm{I}}$ and $(0, 20, 1)_{\mathrm{I}}$ definitely belong to the $P = 22$ polyad. The polyads do not crumble, rather they change their face.

With increasing total energy, more and more isomerization states come into existence in each polyad, and the number of such states rapidly increases. Simultaneously, more and more of the regular states, those that exist at lower energies, disappear. Because the isomerization states have a large anharmonicity, the energetic ordering at the lower end of the polyads becomes complicated and confusing (Figure 8). Actually, without being able to examine the wave functions, it would seem to be impossible to understand the level structure in this energy regime.

Because the isomerization states drop considerably in energy with respect to the top members within a particular polyad, neighboring polyads begin to overlap. The increasing complexity is illustrated in Figure 11 (online only; also available through http://AnnualReviews.org, Electronic Materials); it depicts all wave functions belonging to polyad [[0, 32]]. Starting with $P = 32$, the isomerization states belonging to the $P + 2$ polyads come close in energy to the $(0, P, 0)$ pure overtone states and could possibly perturb them; we return to this point below.

The most important difference between the $(0, v_2, 0)_{\mathrm{I}}$ isomerization states and the $(0, v_2, 0)$ overtone states is that the isomerization states do follow the minimum-energy isomerization path and therefore are not confined to angles close to linearity. This is demonstrated in Figure 12 (online only; also available through http://AnnualReviews.org, Electronic Materials), which shows the wave function for the state $(0, 40, 0)_{\mathrm{I}}$ superimposed on the potential energy contours; the wave function nicely samples the minimum-energy path, including the waist of the peanut. Figure 5 depicts the angle $\gamma_{\max}$, at which the wave function of each $(0, v_2, 0)_{\mathrm{I}}$ state is largest. The contrast with the $(0, v_2, 0)$ states is striking. This picture also demonstrates that the isomerization states come into existence just where the potential energy profile, and therefore the overall structure of the classical phase space, changes rapidly.

The energy spacing Δ_i between adjacent levels within a $v_1 = 0$ polyad steadily increases from the bottom to the top for $P \leq 10$ (Figure 8). However, starting with $P = 12$, Δ_i gradually develops a nonmonotonic behavior, which becomes clearly visible for polyads $P = 14$ and higher: Δ_i is large at the bottom, then decreases, goes through a minimum, and eventually increases again. This general behavior is simply the consequence of the different wave function characters for the states at the bottom and the top of the polyads. A semiclassical analysis of effective Hamiltonian models provides an explanation in terms of quantizing trajectories located on either side of a separatrix (64, 65).

After the isomerization states had been predicted by the calculations using the old, less-accurate PES, they were also found experimentally, however at slightly lower energies (66). What was found in the spectra was a progression of states, which could not be explained by the other progressions analyzed previously and which exhibited an uncharacteristically large anharmonicity and unusually large rotational constants (levels *a–e*, Figure 2). These are exactly the features of isomerization states predicted by Beck et al (42). Now, with the new PES in hand, we can directly compare these particular measured levels with the calculated isomerization states (Table 2), and very good agreement is observed. Definitive assignment of the measured levels is possible only on the basis of the calculations and this almost perfect state-by-state agreement. The isomerization states are true bending states, and therefore they should have at least as good Franck-Condon overlap factors with the intermediate levels in the $\widetilde{A}$ and $\widetilde{C}$ states as do the states belonging to the v_2 progression.

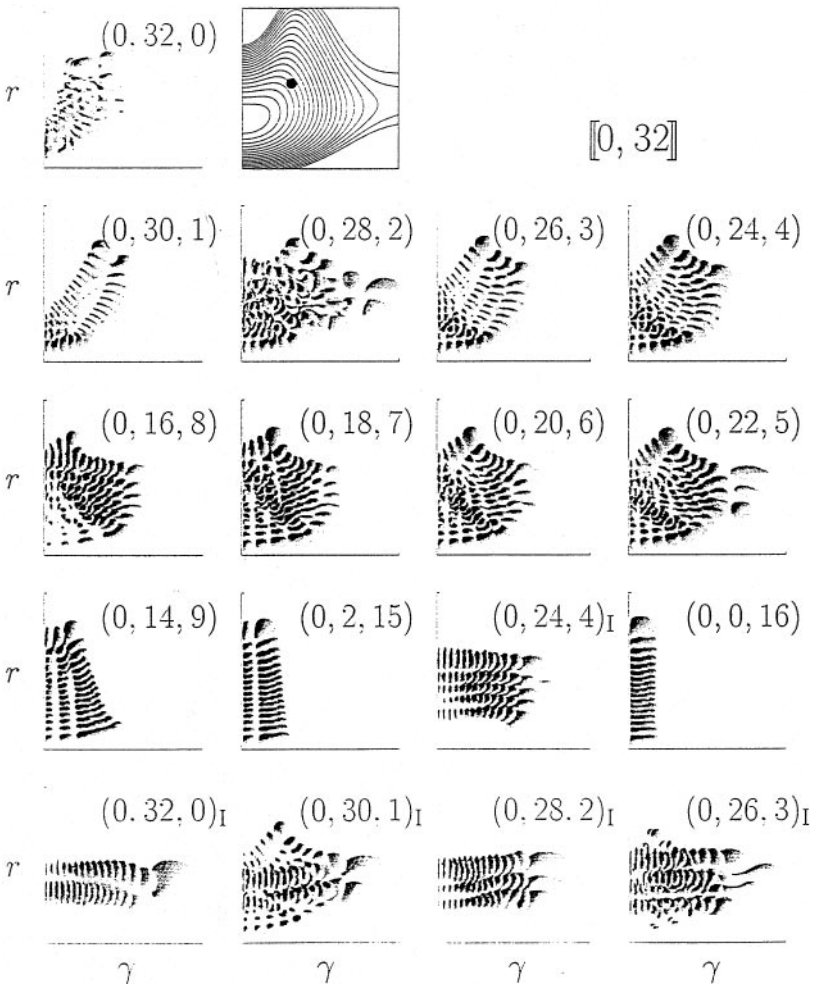

Figure 11 Wave functions for the eigenstates belonging to polyad [[0,32]]. (*Horizontal axis*) Ranges from $\gamma = 180^\circ$ to 100°; (*vertical axis*) ranges from $r = 2.40$ a_0 to 4 a_0.

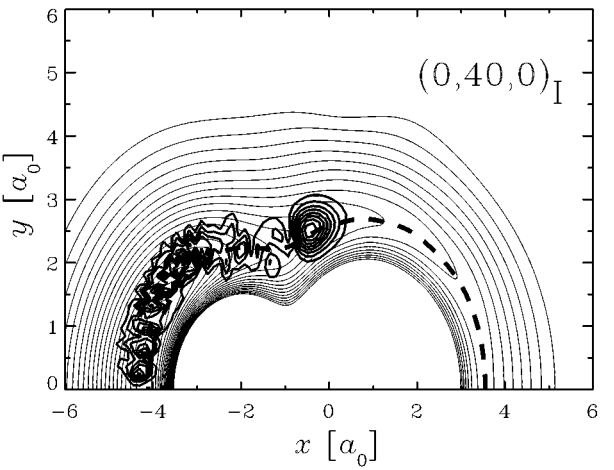

Figure 12 Wave function of the isomerization state $(0,40,0)_{\mathrm{I}}$ superimposed on the potential energy surface. (*Dashed line*) Minimum-energy path.

TABLE 2 Comparison of measured (Exp.) and calculated (QM) vibrational energies and rotational constants B (in cm^{-1}, relative to the ground vibrational state) for the progression of isomerization states $(0, v_2, 0)_I$[a]

v_2	Exp.	QM	B_{Exp}	B_{QM}
22	13424	13425	0.695	0.695
24	14497	14494	0.688	0.698
26	15505	14497	0.723	0.702
28	16413	16393	0.707	0.704
30	17172	17129	0.725	0.711

[a]Experimental data from Reference 66:Table 1.

Polyads for $v_1 \neq 0$

Because of space limitations, we can touch only briefly on how the polyad structure changes when the HC mode is excited, i.e. when $v_1 \geq 1$. As one immediately sees from Figure 8, the polyad structure for $v_1 = 1$ and 2 differs from the structure for $v_1 = 0$. The polyads for $v_1 \geq 1$ are not just replicas of the $v_1 = 0$ polyads merely shifted upward by one quantum of the HC stretch mode. This indicates that the coupling between the HC stretch mode, on the one hand, and the CP stretch mode and mode v_2, on the other, is not negligible. The influence of this coupling is also evidenced by the decrease in the energy gap between the states $(v_1, 2, 0)$ and $(v_1, 0, 1)$ from 59.2 cm^{-1} for $v_1 = 0$ to 22.4 cm^{-1} for $v_1 = 2$ (starting with $v_1 = 3$ the gap increases again). This decrease is mainly caused by the lowering of the frequency of the bending mode with increasing v_1. As a consequence, the 2:1 bend-stretch resonance condition is better and better fulfilled at low P when the HC mode is excited, and this, in turn, results in stronger intrapolyad mixing. The enhanced mixing at low P is clearly exhibited by the corresponding wave functions, which at the lowest energies show the behavior typical of normal-mode states. As the polyad quantum number P increases, the states at the top of the polyad behave identically to the top states in the $v_1 = 0$ polyads, namely they develop more and more CP stretch character. However, the states at the bottom of the polyad acquire increasingly more bending character, and the wave functions behave similarly to the isomerization wave functions discussed in detail for $v_1 = 0$. The most important points to be made here are that this evolution from normal mode to isomerization character occurs at lower values of P and that it is very gradual, i.e. the sudden changes observed to occur for $v_1 = 0$ over a relatively narrow energy range is replaced by a gradual evolution.

A more detailed discussion of the $v_1 \geq 1$ spectra is given by Beck et al (59). Qualitatively, the differences between $v_1 = 0$ and $v_1 \geq 1$ polyads can be explained by two-dimensional adiabatic PESs $\widetilde{V}_{v_1}(r, \gamma)$. They are constructed in an adiabatic way by solving the one-dimensional Schrödinger equation for the HC

stretching degree of freedom, R, for a fixed pair of coordinates r and γ, i.e. the HC stretch mode on the one hand and the combination of the CP stretch and the bending mode on the other are adiabatically decoupled. The eigenvalues obtained by solving the Schrödinger equation define a set of two-dimensional PESs, one for each value of v_1. The minimum-energy paths derived from the $\widetilde{V}_{v_1}(r, \gamma)$ are depicted in Figure 5*b*. Two observations are immediately apparent. First, the angular force constant slightly but noticeably decreases with increasing v_1; this explains the decrease in the bending frequency with increasing HC stretching quantum number and, hence, the systematic change in the quality of the bend:CP stretch resonance condition for $v_1 = 0, 1$, and 2. Second, the change in slope of the isomerization path from the harmonic region at low energy to the more linear γ-dependent branch that occurs near $\gamma \approx 130^\circ$ is less abrupt for $v_1 = 1$ and 2 than it is for $v_1 = 0$. As a consequence, the polyads for $v_1 \geq 1$ evolve more smoothly with the polyad quantum number P. Moreover, as seen in Figure 8, the intrapolyad energy spacing Δ_i changes drastically from $v_1 = 0$ to 1, 2, and 3.

SPECTROSCOPIC HAMILTONIAN

The polyad structure of the energy levels emerges naturally from the quantum mechanical variational calculations performed using the full PES, without any assumptions about the particular form of the PES (Taylor series expansion, for example) or the underlying Hamiltonian; it is an immediate consequence of the 2:1 resonance of the bending and CP stretching frequencies. The energy dependence of the centers of the polyads (average over all polyad components) can be easily described by a three-mode Dunham-type expansion. More interesting, however, is the distribution of levels inside a particular polyad, as this distribution reflects the coupling between the various states that belong to the polyad (22, 67). This intrapolyad structure is most revealing of dynamical details.

In a simplified treatment, which explicitly takes into account the polyad structure and which assumes that P is a "good", i.e. conserved, quantum number, one can define a basis of zero-order wave functions $\Psi^{(P)}$ as products of single-mode wave functions $\phi^{(2)}_{v_2}(\gamma)$ and $\phi^{(3)}_{v_3}(r)$ (the HC stretching mode is omitted in the following discussion and only even values of P are considered),

$$\psi_i^{(P)}(r, \gamma) = \phi^{(2)}_{v_2=P-2i}(\gamma)\, \phi^{(3)}_{v_3=i}(r), \qquad 4.$$

with $i = 0, \ldots, P/2$. Note that $v_2 + 2v_3 = P$. The single-mode basis functions are perfectly aligned along the γ- or the r-axis with $P-2i$ and i nodes, respectively. The true wave functions for the eigenstates that belong to a particular polyad are then expanded as

$$\Psi^{(P)}(r, \gamma) = \sum_i a_i^{(P)} \psi_i^{(P)}(r, \gamma). \qquad 5.$$

Representing the full Hamiltonian in this basis yields the Hamiltonian matrix

$$H_{ii'}^{(P)} = \left\langle \psi_i^{(P)} | \hat{H} | \psi_{i'}^{(P)} \right\rangle \qquad 6.$$

with dimension $(P/2 + 1) \times (P/2 + 1)$. Diagonalization of this matrix gives $P/2 + 1$ eigenvalues, which can be considered as reasonable approximations of the real vibrational levels in this particular polyad. In contrast to the exact procedure, only a very small matrix has to be diagonalized. The price to be paid is the neglect of any coupling between different polyads, regardless of whether they belong to the same or to different values of v_1.

If one assumes that the single-mode wave functions are of the harmonic type and that the PES is expanded in a Taylor series in the coordinates, one can evaluate the elements of the Hamiltonian matrix analytically. The first and therefore most important potential term that contributes to the intra-polyad coupling is $\gamma^2 r$. If the PES is known, the above procedure provides a well-defined recipe for approximately calculating—with modest numerical efforts—the vibrational energies and wave functions (see 68, and references therein). If the potential is not known, which is usually the case, one can parameterize the elements of the Hamiltonian matrix and then determine the unknown parameters by fitting the experimental levels (effective, resonance, or spectroscopic Hamiltonian approach) (21). This requires, of course, that one knows which of the observed levels belongs to the particular polyad and how these levels map onto the totality of levels in a given polyad. In the case of HCP, finding the correct relationship is not difficult for the lower polyads, but once the isomerization states appear, this, because of their large anharmonicity, becomes increasingly difficult at higher energies. In a sense, polyad patterns are the spectroscopist's alternative to direct access to wave functions. Effective Hamiltonians have a long history in molecular spectroscopy (69).

In this section, we describe two fits to the same effective Hamiltonian model: one of the set of calculated data and another of the set of measured energies, however including only states with $v_1 = 0$. (There are no experimentally observed and securely assigned states that have excitation in the HC stretching mode.) The expressions used for the elements of the effective Hamiltonian matrix are

$$\langle v_1, v_2, v_3 | \hat{H} | v_1, v_2, v_3 \rangle = \sum_n w_n v_n + \sum_{n \geq m} x_{nm} v_n v_m + \sum_{n \geq m \geq k} y_{nmk} v_n v_m v_k + z_{2222}\, v_2^4 \qquad 7.$$

for the diagonal elements, and

$$\begin{aligned} \langle v_1, v_2, v_3 | \hat{H} | v_1, v_2 - 2, v_3 + 1 \rangle &= \frac{1}{2\sqrt{2}} \sqrt{v_2^2 (v_3 + 1)} \\ &\times \left\{ k_{223} + \lambda_1 \left(v_1 + \frac{1}{2} \right) + \lambda_2 v_2 + \lambda_3 (v_3 + 1) + \mu_{22} v_2^2 \right. \\ &\left. + \mu_{23} v_2 (v_3 + 1) + \mu_{33} (v_3 + 1)^2 \right\} \end{aligned} \qquad 8.$$

for the off-diagonal elements; remember that the constraint $v_2 + 2v_3 = P$ must be fulfilled. Energy normalization is made with respect to the ground state (0, 0, 0). Recent applications of effective Hamiltonian treatments of highly excited vibrational states by spectroscopists can be found elsewhere (70–74).

In an attempt to evaluate the quality of the effective Hamiltonian model for HCP, the complete set of quantum mechanical energy levels for $v_1 = 0$ up to $P = 30$ are fitted (fit A). One goal is to determine whether the effective Hamiltonian model generates the same qualitative changes in wave functions and other diagnostics as the exact Hamiltonian. When performing the fit, it is essential to reproduce both energy positions and the assignments $[v_1, P, i]$, where i indicates the position of the level inside the polyad (top state $i = 0$, bottom state $i = P/2$). The adjusted parameters are listed in Table 3 (online only; also available through http://Annual Reviews.org, Electronic Materials).

In Table 1 (online only; also available through http://AnnualReviews.org, Electronic Materials), we compare the fitted energies from the polyad Hamiltonian with the exact ones from the full Hamiltonian for four different polyads. The root mean square deviations are 2.1, 2.5, 4.1, and 6.0 cm^{-1}, respectively. As expected, the accuracy of the fit is very good for the lower polyads but diminishes with increasing polyad quantum number. For $P = 30$, the agreement is worst at the lower-energy end of the polyad, where because of the isomerization states (or interpolyad interactions) the deviations from the "normal" behavior are most significant. Nevertheless, it is astonishing how well the model reproduces even the disordering caused by the occurrence of the I states.

Fitting the vibrational energies is, however, only half of the success story; the wave functions are also well reproduced by the model Hamiltonian. For example, the wave functions for polyad [[0, 32]] obtained from the model Hamiltonian (not shown here) compare well with their counterparts in Figure 11 (online only; also available through http://AnnualReviews.org, Electronic Materials), even though this polyad was not included in the fitting procedure. The general structures, qualitative changes, and even finer details are astonishingly well reproduced. The admixtures from other polyads, clearly seen in the exact wave functions, are, of course, not mimicked by the isolated polyad model calculations. Because the mixing between states belonging to different polyads increases rapidly with P, the effective Hamiltonian model would have to be significantly extended, by inclusion of several interpolyad interaction mechanisms for applications above $P \approx 34-36$ or so (75).

A satisfactory fit of the complete set of calculated energy levels is necessary to confirm that the effective Hamiltonian model is capable of describing the structural changes observed in the lower-energy regions of each polyad. More interesting and significantly more difficult, however, is the question of whether the effective Hamiltonian model can also correctly describe the experimental energy levels. The list of experimental data is incomplete; with increasing polyad quantum number, more and more levels in the lower-energy region of each polyad have not been observed experimentally. Moreover, the measured spectrum yields only indirect

TABLE 3 The parameters obtained in fits of the calculated (fit A) and the measured (fit B) energy levels [a]

Fit	ω_2^0	ω_3^0	x_{22}^0	x_{23}^0	x_{33}^0	y_{222}^0	y_{223}^0	y_{233}^0	y_{333}^0
A	678.14	1289.86	−5.002	−5.523	−5.877	0.2385	0.0330	0.0427	−0.0103
B	679.01	1284.09	−4.935	−4.982	−5.565	0.2255	0.0065	0.0698	−0.0358

Fit	z_{2222}^0	$k_{223} + \lambda_1/2$	λ_2	λ_3	μ_{22}	μ_{23}	μ_{33}	# of data	σ
A	−0.00624	14.71	−0.0639	−1.193	0.0067	0.0083	0.0326	135	4.84
B	−0.00590	12.51	0.2794	−1.1858	−0.0069	0.0151	0.0298	82	8.31

[a] All values are in units of cm^{-1}.

(through rotational constants and relative intensities) and therefore vague information about the shapes of the wave functions and thus about assignments. Both shortcomings make the effective Hamiltonian model more difficult to apply. In fact, it would be hopeless to apply the polyad model to experimental data were it not for the ability to bootstrap from many securely assigned and simultaneously fitted polyads to the level patterns (spacings, intensities, rotational constants, vibrational fine structure) of the next-higher polyad. However, the assignment process begins to break down as soon as one incorrect correspondence between observed and calculated levels is incorporated into the bootstrap process.

In an attempt to model the experimental data, Ishikawa et al (36) made an effective Hamiltonian fit to the observed vibrational levels without using any information derived from quantum mechanical energy-level calculations (which were not available for the new PES when the fits were performed). Although the lower polyads and the top parts of the higher polyads—where the isomerization states and the onset of overlap between $[[0, P]]$ and $[[0, P + 2]]$ polyads do not complicate the spectral patterns—are quite well described, the lower ends of the higher polyads are in substantial disagreement with the new calculations. This is not surprising because the available experimental information is not sufficient to guarantee valid extrapolation to unobserved levels.

With the new calculations in hand, the same experimental data have been fitted once again, this time, however, taking into consideration information relevant to the assignments derived from the full quantum mechanical calculation. No calculated levels are included in this fit; the calculations are used exclusively to ensure that each observed level is assigned to the correct polyad eigenstate. The results of this fit (fit B), in which energies up to $P = 36$ are included, are also listed in Table 1 (online only; also available through http://AnnualReviews.org, Electronic Materials) and the agreement with the theoretical data is reasonable. Energies of levels that have not been measured are predicted in an acceptable manner by the model. Although the fit of the (incomplete) set of experimental energies is good, we must emphasize that in some cases the deviations from the calculated energies, which in this energy regime are believed to be still trustworthy, are large (e.g. state no. 328). In addition, looking at the wave functions calculated from the fit of the experimental data, one occasionally notices a wrong assignment, especially at the lower end of the polyad.

CLASSICAL MECHANICS APPROACH

Although the full quantum mechanical calculations provide enormous detail about the spectrum and how the wave functions evolve with energy, the overall picture would be incomplete without being accompanied by classical mechanics calculations, i.e. an analysis of the structure of the corresponding classical phase space (9). In numerous applications it has been demonstrated that classical trajectories, the solutions of Hamilton's equations of motion, provide valuable insights into the

intra- and intermolecular dynamics (76). Owing to the richness of detail generated by the exact quantum mechanical calculations, deeper insights require guidance from classical mechanics. This is particularly true for the highly excited states, which may be governed by nonlinear dynamics effects (77).

Of particular importance for understanding the structure of the classical phase space, and hence the dynamics of a (rotationless) molecule, are periodic orbits (POs), i.e. closed trajectories in the $(2N-1)$-dimensional phase space for a given energy E (9, 25, 26, 78). If the initial conditions for the coordinates and momenta of a trajectory lie on a PO, the system remains on this particular orbit for all times. One distinguishes between stable and unstable POs. An orbit is called stable if trajectories, which are initiated in the vicinity of this PO, stay close to it for all time. Likewise, an orbit is called unstable when all trajectories launched in the neighborhood of the PO exponentially depart from that orbit (like the motion of a billiard ball on a potential ridge). POs provide the structure of the classical phase space and—in a loose sense—they are the backbones for the quantum mechanical wave functions, i.e. the wave functions are localized around the POs (scarring of wave functions) (79, 80). Finding POs for a system with more than two degrees of freedom is not simple. Numerical methods have been developed, but they are not routine, especially at high energies (81, 82).

POs have been calculated for HCP at many fixed energies, from the bottom of the well up to more than 3 eV. At low energies one finds three different families of POs, the so-called principal families, which are denoted as [B], [r], and [R], respectively. An example of a PO for each family is superimposed on the corresponding potential contour diagrams in Figure 6. The orbits that belong to the [R] and [r] families are confined to the plane $\gamma = 180^\circ$ and describe primarily motions along the R- and r-axes, respectively (Figure 6*e* and *f*). The orbits belonging to the [B] family explore the full three-dimensional coordinate space. At very low energies they perform oscillations basically along the angular coordinate, and that is the reason we term them bending (B) orbits. However, just like the quantum mechanical wave functions, the [B]-type trajectories quickly become dominated by CP stretching character as the energy increases (Figure 6*a* and *c*). The angular region explored by these trajectories remains confined to a small interval ($\Delta\gamma \approx \pm 40^\circ$) around the linear configuration. The comparison of [R], [r], and [B] POs with the quantum mechanical wave functions of the $(v_1, 0, 0)$, $(0, v_2, 0)$, and $(0, 0, v_3)$ pure progressions clearly demonstrates the correspondence between classical and quantum mechanics.

Instead of plotting and analyzing many individual POs, one can obtain a comprehensive overview of the structure of the classical phase space by so-called continuation/bifurcation diagrams (83). This is nothing more than a plot of one particular quantity (e.g. the maximum value of a coordinate, the period of the orbit, etc) for each family of POs plotted as a function of the energy. Continuation/bifurcation diagrams are direct fingerprints of the (classical) dynamics of the system. They call attention to those energy regimes in which interesting qualitative changes both in the classical dynamical and in the quantum mechanical worlds

occur. Other examples of continuation/bifurcation diagrams can be found elsewhere (84–88).

In Figure 9*b* we show an example of a continuation/bifurcation diagram. Plotted are the frequencies ($\nu = 2\pi$/period, in energy units) of the various types of POs versus energy. Each point in this figure corresponds to one PO. All three of the principal families, [B], [r], and [R], are robust. In other words, the orbits are stable and can be followed without ambiguity up to high energies. (The curve for the [R] family is not shown here.) The [B] family exhibits a bifurcation into two branches at $E = 1.338$ eV. However, the periods as well as the general structure of the two corresponding POs are so similar that quantum mechanics does not distinguish between them, i.e. both orbits can be considered as backbones of the $(0, P, 0)$-type wave functions.

The most interesting feature of the classical trajectory study is another bifurcation, a so-called saddle-node bifurcation at $E = 1.669$ eV. At this energy, a new family of POs, which we refer to as the [SN1] family, suddenly comes into existence. [SN1] POs do not exist at lower energies—they are abruptly born at the bifurcation. The [SN1] bifurcation is not a bifurcation of the [r] branch, as Figure 9 might suggest. An example of a [SN1]-type PO is depicted in Figure 6*b* and *d*. In contrast to the [B]-type orbits, a [SN]-type PO extends to larger angles and clearly follows the minimum-energy isomerization path. However, at higher energies, the [SN1] POs also stop penetrating deeper into the CP–H hemisphere and are deflected away from the minimum-energy path. This development is accompanied by an abrupt bend of the frequency curve at around 2.1 eV. But near this energy another saddle-node bifurcation occurs at 2.164 eV, [SN2], and the corresponding orbits for this new family of POs do continue to follow the isomerization path. At still higher energies, more and more [SN]-type POs are born, which penetrate deeper and deeper into the CP–H hemisphere of the PES. However, locating them becomes increasingly problematic. The [SN]-type POs are the classical backbones for the wave functions for the $(0, v_2, 0)_{\mathrm{I}}$ family of states that we have called isomerization states.

The close resemblance of the frequencies of the various types of POs with the analogous quantum mechanical transition frequencies is another manifestation of the classical/quantum mechanical correspondence principle—despite the slightly different horizontal axes shown in Figure 9*a* and *b*. The isomerization states $(0, P, 0)_{\mathrm{I}}$ first seem to follow the [SN1]-type POs up to the kink of the [SN1] frequency curve. At higher energies, the wave functions are then guided by the [SN2] POs. At still higher energies, where more and more saddle-node bifurcations occur, the picture becomes much more complicated, and a clear-cut correspondence between POs and wave functions is no longer obvious. This is in accord with the observation that pure $(0, P, 0)_{\mathrm{I}}$ states cannot be located beyond $P = 40$. At these high energies, the coupling between the internal modes is apparently so strong that many of the wave functions have no readily assignable nodal structure.

SEMICLASSICAL APPROACH

The classical approach briefly described in the previous section is able to explain some of the coarser features of the quantum mechanical calculations, such as the general nodal structure of the wave functions and the occurrence of qualitatively new families of states. Classical mechanics is, however, not suited for answering more subtle questions, such as why the isomerization states come into existence in the lower-energy region of the polyads and not at the top, why the I states and the CP stretching states are interleaved ($P = 22$ in Figure 10), or why the general behavior is different for $v_1 = 0$ versus $v_1 = 1$? In order to answer such questions, a semiclassical theory is needed, in which each quantum level corresponds to one particular classical trajectory [Einstein-Brillouin-Keller (EBK) quantization] (89). Because a semiclassical theory for a three-mode system with an arbitrary PES is difficult to formulate, one uses a much simpler but approximate Hamiltonian as the starting point for a semiclassical analysis. This approach has the advantage that approximate constants of motion or good quantum numbers can be built in from the beginning. If a resonance phenomenon governs the spectrum, a spectroscopic effective Hamiltonian is the natural choice. Because of lack of space, only some flavor of the semiclassical approach can be given here; for more details see Joyeux et al (65, 90 and references therein).

The classical analogue of the 2:1 stretch-bend resonance Hamiltonian, which can be rigorously derived from perturbation theory (91, 92), is given by $H = H_{\mathrm{D}} + H_{\mathrm{F}}$ (D and F stand for Dunham and Fermi, respectively), where

$$H_D = \sum_n \omega_n I_n + \sum_{n \geq m} x_{nm} I_n I_m + \sum_{n \geq m \geq k} y_{nmk} I_n I_m I_k + \cdots \qquad 9.$$

and

$$H_F = I_2 \sqrt{I_3} \cos(2\varphi_2 - \varphi_3) \left(k + \sum_n \lambda_n I_n + \cdots \right). \qquad 10.$$

The I_n and φ_n ($n = 1{-}3$) are action/angle variables (68). (φ_1, I_1), (φ_2, I_2), and (φ_3, I_3) approximately correspond to motion along R, γ, and r, respectively. Note the formal similarity of Equations 7 and 8, on the one hand, with Equations 9 and 10, on the other. The constants ω_n, x_{nm}, etc, can be obtained either directly from the PES, provided a Taylor series expansion of the potential around the equilibrium is sufficiently accurate, or by fitting the energy levels of the full quantum mechanical calculation, as described above. In this work, the latter procedure is used, including all energy levels up to about 18,700 cm^{-1} above the lowest one; states with $v_1 \neq 0$ are not excluded. The approximate wave functions are observed to closely resemble the exact ones. Details are given by Joyeux et al (90).

For the subsequent discussion, it is convenient to make the following additional transformations: $\psi = \varphi_2 - \varphi_3/2$, $\theta = \varphi_2$, $J = 2I_3$, and $I = I_2 + 2I_3$, where the angles ψ and θ are conjugate to J and I, respectively. Deriving the classical

equations of motion for the coordinates φ_1, ψ, and θ and for the generalized momenta I_1, I, and J, it immediately follows that

$$\frac{dI_1}{dt} = \frac{dI}{dt} = 0, \qquad 11.$$

i.e. I_1 and I are constants of motion and, according to the EBK quantization rules, can be set to $v_1 + 1/2$ and $P + 2$, respectively. (The additional terms $1/2$ and 2 in the relationship between I_1 and I and the quantum numbers v_1 and P are Maslov indices.) The only nontrivial equations of motion concern ψ and J. The corresponding quantization condition reads

$$\mathcal{J}_J \equiv \frac{1}{2\pi} \int_{\psi \in [0,\pi]} J \, d\psi = n + \frac{1}{2}, \qquad 12.$$

where $\mathcal{J}_J$ is the action integral and $n = 0, \pm 1$, etc. Because two of the generalized momenta, I_1 and I, are conserved, the classical resonance Hamiltonian can be treated as an effective one-dimensional problem. In particular, trajectories can be calculated and analyzed for any specified quantum polyad $[[v_1, P]]$. Such a simplification is definitely impossible in the full classical approach. The advantages of this reduced dimensionality picture are as follows: First, the classical equations of motion can be solved analytically; second, POs can be determined for any pair of quantum numbers v_1 and P; and third, the original three-dimensional semiclassical quantization condition is reduced to a one-dimensional root-search procedure.

We are now in a position to answer the detailed questions raised at the beginning of this section. Similar to the full classical approach, however, one can calculate POs now for any specified values of v_1 and P rather than for fixed energy. The corresponding energies of the different families of POs are plotted versus P (not necessarily an integer) in Figure 13*a*, where $v_1 = 0$ is chosen for this example. Figure 13*b* shows, on an expanded energy scale, the same data but centered around the energy of the [r]-type PO, so that the details are more visible and understandable. Up to $P = 12$ one finds only two POs, one that approximately corresponds to the CP stretch, [r], and one that corresponds to the bending motion, [B]. A saddle-node bifurcation occurs at $P = 12.297$, corresponding to an energy of 10,732 cm^{-1} relative to the quantum mechanical ground state (corresponding to 1.699 eV above the bottom of the potential well), where [SN]-type POs, which have the same general behavior as in the full classical calculations, suddenly appear. Actually, two branches of [SN]-type orbits are born at the saddle-node bifurcation, a stable one, labeled [SN], and an unstable one, labeled [$\overline{\text{SN}}$]. The unstable POs also exist in the classical treatment, but they have not been followed.

The semiclassical energies, E_i ($i = 0, 1, \ldots, P/2$), for each specified value of P (which, incidentally, agree perfectly with the corresponding quantum mechanical energies obtained from the fit) lie in the classically allowed region between the [B] curve and the [r] or [SN] curves. These energy values are determined by the quantization condition in Equation 12. The energy where the bifurcation occurs

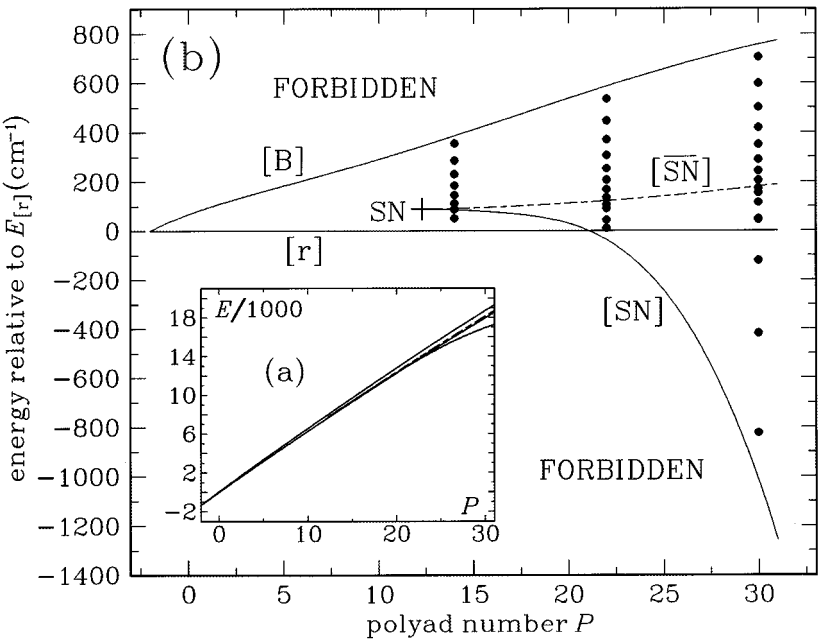

Figure 13 (*a*) Energies of the four different periodic orbits (with respect to $E = 0$ at the quantum mechanical ground state energy) derived from the spectroscopic Hamiltonian, Equations 9 and 10, as functions of the polyad quantum number P; the HC stretching quantum number is $v_1 = 0$. (*b*) The same as in (*a*) but on an expanded energy scale, with respect to the energy of the [r] PO. [r], [B], and [SN] indicate the different families of periodic orbits. (*Dashed curve*) The unstable periodic orbit that appears simultaneously with the [SN]-type orbits at the saddle-node (SN) bifurcation. (*Heavy dots*) The semiclassical energies E_i for $P = 14$, 22, and 30 obtained from the quantization condition Equation 12.

lies close to the [r] curve, which implies that the metamorphosis of the normal states into isomerization states initially occurs at the lower end of the polyads, just as is observed for the quantum mechanical wave functions shown in Figure 10. However, the energy of the bifurcation lies slightly inside the classically allowed region, not directly on the [r] curve, which explains why the qualitative change of the wave functions first appears in the second-lowest state and not in the lowest one. The curves in Figure 13 also predict very nicely that for the higher polyads, for example $P = 30$, the three lowest levels must lie considerably below the energy of the pure CP stretching level.

The CP stretch and isomerization state wave functions for the [[0, 22]] polyad show a surprising alternating behavior at the bottom of the polyad (Figure 10);

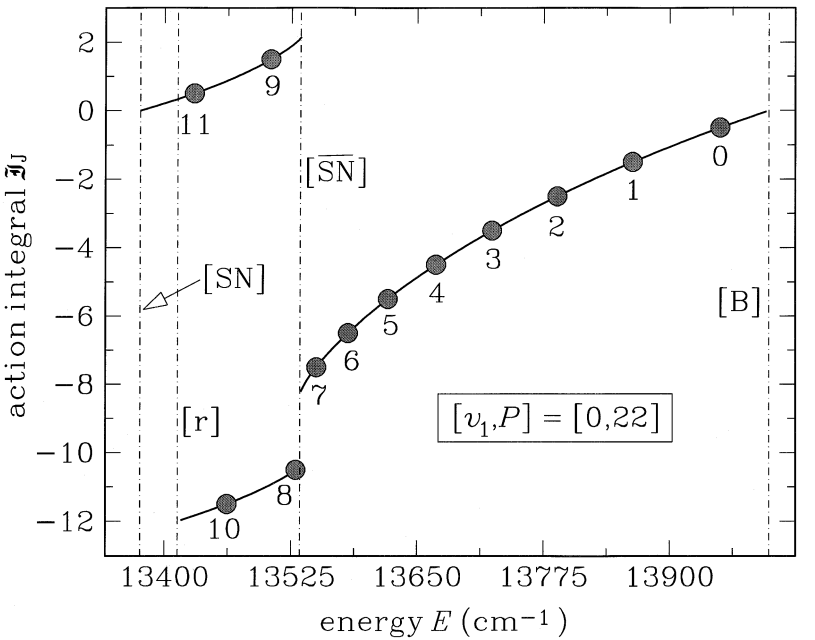

Figure 14 The classical action integral $\mathcal{J}_J$ as a function of energy (normalized to the quantum mechanical ground state energy) for polyad [[0, 22]]. (*Vertical lines*) The energies for the four periodic orbits [r], [B], [SN], and [$\overline{\text{SN}}$]; (*heavy dots*) the semiclassical energies E_i obtained from the quantization condition Equation 12; E_0 is the energy of the highest level in this polyad and E_{11} is the energy of the lowest one.

similar behavior is also found for higher polyads [see the wave functions for polyad [[0, 32]] in Figure 11 (online only; also available through http://AnnualReviews.org; Electronic Materials)]. This peculiar observation can be explained by analyzing the quantization condition. In Figure 14, we plot, for the [[0, 22]] polyad, the action integral, $\mathcal{J}_J$, as a function of energy. The vertical lines indicate the energies of the four POs present at this energy. The essential feature is the splitting of $\mathcal{J}_J(E)$ into two branches in the low-energy range. The different values of $\mathcal{J}_J$ for the two branches indicate that the two branches represent qualitatively different motions. The trajectories belonging to the upper branch are of the I type, whereas those for the lower branch have mainly CP stretch character. The trajectories, which are relevant for the quantum mechanical dynamics, are those for which the quantization condition is fulfilled. Thus, although for $i = 0$–7 all trajectories lie on the same curve, the energetic ordering of trajectories 8–11 is interleaved: 8 and 10 belong to the normal branch, and 9 and 11 belong to the other one. Additional examples of semiclassical studies based on effective Hamiltonians can be found elsewhere (e.g. 30, 93–100).

SPECTROSCOPIC PERTURBATIONS

Up to now we have only discussed the vibrational spectrum up to moderate excitation energies, $P \leq 30$. With increasing energy, the structure of the spectrum becomes rapidly more intricate. Because the frequency (i.e. consecutive level spacing) of the isomerization states is significantly smaller than are the frequencies of the $(0, v_2, 0)$ and $(0, 0, v_3)$ states, and because more and more members of the lower half of each polyad turn into I states, the number of $(v_1, v_2, v_3)_I$ states increases rapidly with energy. As a result of their relatively small frequency, isomerization states belonging to higher polyads begin to overlap the energy region of the normal states at the top of lower-P polyads (Figure 8). Thus, one expects interpolyad interactions to affect the states observed in the SEP spectra. Moreover, mixing between polyads belonging to different values of the HC stretch quantum number also generally becomes more likely, again because of overlapping energy regions. As a result, increasingly fewer states can be clearly assigned based on the nodal structure of their wave functions. The examples for $P = 32$ in Figure 11 (online only; also available through http://AnnualReviews.org, Electronic Materials) illustrate this general behavior.

In the SEP experiment of Ishikawa et al (40), the pure $(0, v_2, 0)$ progression was followed from $v_2 = 26$ up to 42. This was possible because the states in this progression are very robust and the wave functions preserve their distinct identity, although small perturbations due to mixing with nearby states do occur for the higher members. In the SEP experiments, only a narrow energy window of width $\Delta E \approx \pm 20\ cm^{-1}$ centered around the predicted $(0, v_2, 0)$ energy was scanned with the probe laser, and the following observation was made: Although for $v_2 \leq 30$ only one vibrational band was observed within the window, starting with $P = 32$ suddenly more than one vibrational state was present. This was interpreted as a "sudden onset of spectroscopic perturbations."

Exactly the same effect is observed in the quantum mechanical calculations. Vibrational states that are quasi-degenerate with the pure $(0, v_2, 0)$ levels exist below the energy of $v_2 = 32$, but these quasi-degenerate levels always have several quanta in the v_1 mode and therefore would not appear in the SEP spectrum because of Franck-Condon selectivity against $v_1 > 0$ levels. However, at $P = 32$, suddenly other vibrational states are predicted to occur in the spectrum near the $(0, v_2, 0)$ states. These states have no excitation in the HC mode and therefore presumably have nonnegligible Franck-Condon intensities. They have mostly the character of isomerization states, which become more and more numerous at $P > 30$. Manifestations of the mixing between normal states of one polyad and the isomerization states belonging to a higher polyad can be seen in Figure 11 (online only; also available through http://AnnualReviews.org, Electronic Materials) for the states (0, 28, 2) and (0, 22, 5) of the $P = 32$ polyad. As a matter of fact, all states $(0, v_2 \leq 30, 0)$ are extremely pure, whereas the wave functions for states $(0, v_2 \geq 32, 0)$ increasingly frequently exhibit admixtures of one or more isomerization states.

Other candidates for anharmonic (as opposed to Coriolis) perturbers of the pure $(0, v_2, 0)$ states are levels with two quanta of HC stretch. As mentioned previously, a weak $2\nu_1$:$10\nu_2$ resonance is already evident at very low vibrational energy. Because ν_1 gradually changes with increasing polyad quantum number, starting with $v_2 = 28$, states with two quanta of excitation of the HC stretch mode are near-degenerate with the pure $(0, v_2, 0)$ states (see Figure 8). An example of such an interpolyad mixing is recognized in Figure 11 (online only; also available through http://AnnualReviews.org, Electronic Materials).

On the other hand, swapping of two quanta of the HC stretching mode for 10 quanta of mode 2 is a very high-order anharmonic process, and therefore we believe that the isomerization states are the more likely candidates for most of the extra states observed in the proximity of the v_2 overtones. Because isomerization states indeed have been observed at lower energies (see Table 2), there is no reason why they should not appear in the SEP spectra at higher energies as well. Several of the additional states have unusually large rotational constants, B, and, as we discuss in the next section, large rotational constants are a signature of isomerization states.

Unfortunately, the limited accuracy of the PES does not allow us to specify uniquely which states, in addition to the main polyad states, are observed in the SEP spectra. The $(0, v_2, 0)$ states are accurately predicted by the calculations, but the high overtones of the I states very likely do not have the necessary predictive accuracy. Nevertheless, the onset of the perturbations is correctly prognosticated.

ROTATIONAL CONSTANTS

Spectroscopists do not have direct access to the wave functions; thus they do not have direct access to the structure of the molecule in a particular vibrational state. The best source of such information, in addition to intensities, is rotationally resolved spectra. In order to extract this information from the rotational-level structure of a linear molecule, an effective Hamiltonian matrix is employed, which is defined by a rotational constant, B, and several vibrational fine-structure constants, g_{22}, q_2, and γ_{ll} (40). The vibrational fine structure arises because the bending mode of a linear triatomic molecule is doubly degenerate; hence, the bending overtones form quasi-degenerate groups of $v_2 + 1$ (v_2 even) or v_2 (v_2 odd) levels, where the levels in each group are distinguished by the vibrational angular momentum quantum number, l (denoted as K in this paper). The degeneracy of the different l components of a given v_2 is lifted in first-order perturbation theory by quartic and sextic anharmonicity effects and in second-order perturbation theory by cubic and quintic anharmonicity and Coriolis effects. This is a complex subject treated in detail by Nielsen (69) and in summary by Mills (101). The two important points are as follows: (*a*) The built-in quasi-degeneracy confers high sensitivity to specific features of the energy-level spectrum, in particular the systematic energy difference between the centers of different polyads such as $[[0, P]]$, $[[1, P - 5]]$,

[[2, $P-10$]], etc. (*b*) The rotational constant does not have its nominal mechanical significance as the expectation value of a reciprocal moment of inertia. Moreover, none of the vibrational fine-structure constants, in particular g_{22}, has a simple mechanical definition. Despite the complexity of the definition of B, g_{22}, etc, considerable insight is gained by examining their behavior versus v_2 as the isomerization states appear and, at higher energies, when the $(0, v_2, 0)$ states tune through degeneracy with states that are excited in the HC stretch mode ($v_1 > 0$).

There are two distinct ways of computing B values in the full quantum mechanical calculations for any vibrational state (v_1, v_2, v_3):

$$B_{\text{spec.}} = \frac{1}{2}[E(1,0) - E(0,0)] \qquad 13.$$

and

$$B_{\text{mech.}} = \left\langle \Psi_{J=0} \middle| I_b^{-1} \middle| \Psi_{J=0} \right\rangle. \qquad 14.$$

The $E(J, K)$ are the energies for rotational quantum numbers J and K, as calculated with the full Hamiltonian, including the Coriolis coupling term, i.e. the last term in Equation 3. $\Psi_{J=0}$ is the vibrational wave function for total angular momentum $J = 0$, and I_b^{-1} is the inverse of the moment of inertia with respect to the *b* rotation axis in the principal axis system. $B_{\text{spec.}}$ includes both anharmonic and Coriolis effects and reflects details incorporated in the effective Hamiltonian used by spectroscopists to extract a fitted B value (e.g. effects of the q_2 parameter as well as off-diagonal intrapolyad interactions and the local effects of specific isolated perturbers). $B_{\text{spec.}}$ is the calculated constant most closely related to the rotational constant extracted from the SEP experiments. $B_{\text{mech.}}$ is an approximation; it involves only $J = 0$ wave functions and therefore does not contain $\Delta K = \pm 1$ coupling effects. However, because $B_{\text{mech.}}$ is an expectation value and thus reflects the average structure of the molecule in a particular vibrational state, it can be exploited to interpret the state dependence of the rotational constant (except for effects that cannot be reflected in $B_{\text{mech.}}$).

It is instructive to compare the computed values of $B_{\text{spec.}}$ and $B_{\text{mech.}}$ with each other, as well as with the B values obtained from the SEP spectrum. It is also instructive to look at the evolution of the spectroscopic values of g_{22} and q_2 (40). The former is sensitive to many of the anharmonic effects that appear in both $B_{\text{spec.}}$ and $B_{\text{mech.}}$ but not at all to the Coriolis effect that appears in $B_{\text{spec.}}$; the latter is sensitive exclusively to the interpolyad Coriolis effects.

In Figure 15*a* we depict the computed and measured B values for the $(0, P, 0)$, $(0, 0, P/2)$, and $(0, P, 0)_{\text{I}}$ progressions in order to illustrate the different behaviors. $B_{\text{mech.}}$ is a useful discriminant for excitation in CP stretch versus bend. Because the CP-extended turning point is much softer than the CP-compressed turning point, excitation of CP stretch causes $B_{\text{mech.}}$ to decrease, typically $\sim$0.003 cm^{-1} per v_3. Because both bending turning points bring the H atom closer to the inertial *b*-axis, a normal bend should cause $B_{\text{mech.}}$ to increase, $\sim$0.0004 cm^{-1} per v_2 at low values of v_2. However, as discussed in detail above, mode 2 acquires more and more the

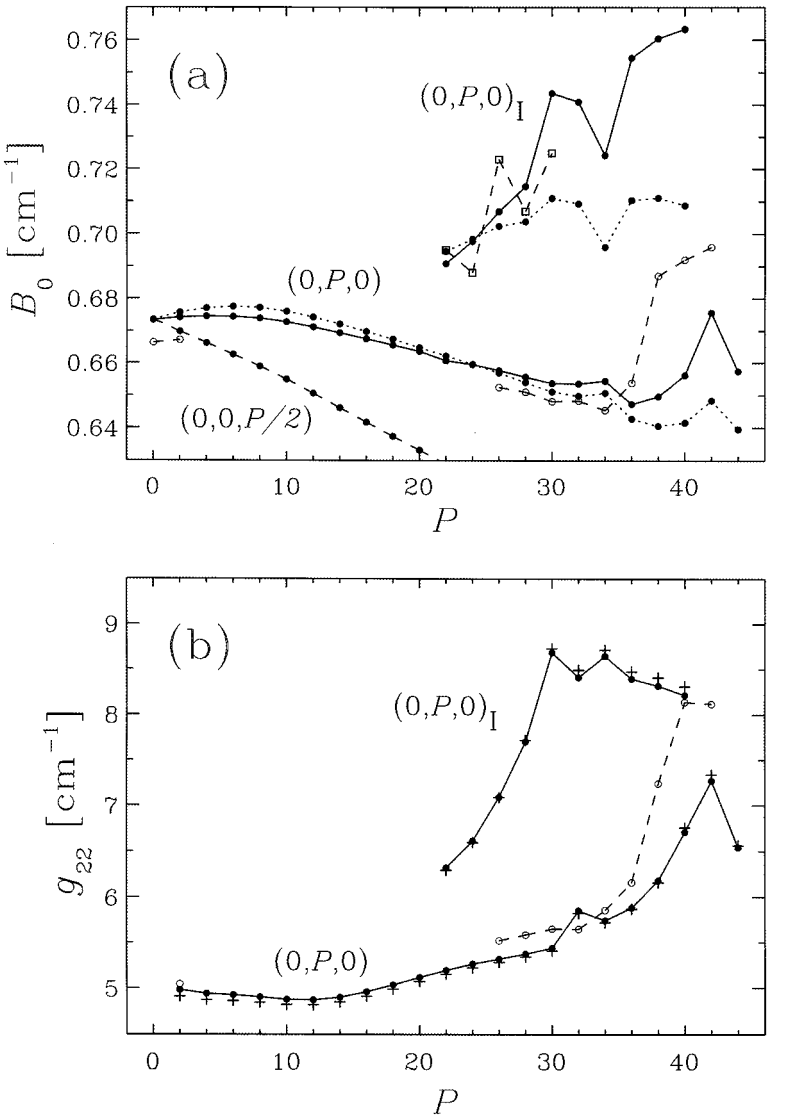

Figure 15 (*a*) Rotational constants B for the three progressions $(0, P, 0)$, $(0, 0, P/2)$, and $(0, P, 0)_{\mathrm{I}}$. (*Open symbols*) The experimental values extracted from the stimulated emission pumping experiments; (*solid lines*) the calculated values $B_{\mathrm{spec.}}$; (*dotted lines*) the values calculated from the moment of inertia, $B_{\mathrm{mech.}}$. (*b*) Experimental (*open circles*) and calculated (*closed dots*) vibrational fine-structure constants g_{22} for the two progressions $(0, P, 0)$ and $(0, P, 0)_{\mathrm{I}}$. (*Crosses*) Values calculated without including the Coriolis interaction term.

character of CP stretch and as a result the B value starts to decrease after going through a maximum around $v_2 = 6$. This decrease continues up to $v_2 = 36$ in the calculation and up to $v_2 = 34$ in the values measured in the SEP spectrum. Owing to their large-amplitude bending motion, the isomerization states are characterized by distinctively large B values. The five experimental values for the $(0, P, 0)_{\mathrm{I}}$ progression in Figure 15*a* show fluctuations, which probably reflect numerical uncertainties arising from incompleteness of the deperturbation model. Although $B_{\mathrm{mech.}}$ approximates $B_{\mathrm{spec.}}$ remarkably well up to $v_2 \sim 36$ for the $(0, P, 0)$ states, discrepancies between $B_{\mathrm{mech.}}$ and $B_{\mathrm{spec.}}$ become substantial above $v_2 \sim 28$ for the progression of isomerization states. The reason is that the description in terms of an averaged moment of inertia apparently breaks down for the large-amplitude bending motion (i.e. maximal classical Coriolis forces), which is characteristic for the $(0, P, 0)_{\mathrm{I}}$ states.

Figure 15*b* shows the other constant, g_{22}, versus P for the two progressions $(0, P, 0)$ and $(0, P, 0)_{\mathrm{I}}$. The calculated values are determined from (40)

$$g_{22} = \frac{1}{4}[E(2, 2) - E(2, 0)] + B. \qquad 15.$$

Because of the linear equilibrium geometry of HCP, there is no meaningful expression for g_{22} in terms of averaged moments of inertia, and therefore we cannot relate the differences in the various progressions or the variations with P to the molecular structure in the specific vibrational states. (In the case of the bent molecule HCO, g_{22} corresponds to the A rotational constant, which approximately corresponds to rotation of the hydrogen atom about the CO axis.) As for the rotational constant B, g_{22} is substantially larger for the isomerization states than for the normal $(0, P, 0)$ states. g_{22} is exclusively controlled by anharmonic coupling terms contained in the PES and not by Coriolis coupling effects. Calculations with and without the last term in the Hamiltonian in Equation 3 give almost identical results; the changes in g_{22} are on the order of $\sim$0.1 cm^{-1}.

The most noticeable features in Figure 15*a* and *b* are the pronounced maxima for the measured B and g_{22} values around $P = 40$; the other vibrational fine-structure constants, q_2 and γ_{ll}, show similar variations with P. In fact it was the appearance of the large B perturbations and large B-values for $(0, P, 0)$ levels that originally provoked the close experimental/theoretical collaboration. The calculated values $B_{\mathrm{spec.}}$ and g_{22} show a similar P dependence, but the maxima are less pronounced compared with their experimental counterparts.

Such resonance-like behavior is symptomatic of interpolyad interactions. When the centers of two families of polyads tune through degeneracy, the magnitudes of the second-order corrections to the B value and to the other vibrational fine-structure constants go through a maximum and the signs reverse (because the energy denominator crosses through zero), leading to an abrupt reversal of trend. The questions to be answered are then (*a*) which states perturb the $(0, P, 0)$ states and (*b*) what is the nature of the perturbation, anharmonic coupling, or Coriolis $\Delta K = \pm 1$ coupling?

As discussed above, there are (at least) two types of possible perturbers. Because of the approximate $1\nu_1$:$5\nu_2$ resonance, states $(1, P-5-2v_3, v_3)$, $(2, P-10-2v_3, v_3)$, etc, tune through resonance with the $(0, P, 0)$ states at larger values of P. The former are coupled by $\Delta K = \pm 1$ Coriolis coupling to the $(0, P, 0)$ states, and the latter perturb the $(0, P, 0)$ states through anharmonic coupling. In addition to these states with excitation of HC stretch, states with strong isomerization character, which emerge from the lower regions of higher polyads, are observed to mix with the $(0, P, 0)$ states. Unfortunately, these isomerization states do not have a clear-cut nodal structure, and therefore they cannot be assigned in terms of quantum numbers; in other words, it is difficult to decide from the exact energy levels and wave functions whether the basis states form a regular progression that tunes through perfect degeneracy with the $(0, P, 0)$ basis states.

The constant g_{22} is not affected by Coriolis coupling, and therefore the perturbations must be caused by coupling through the PES. The small glitch in g_{22} at $P = 32$ is probably due to a resonance with state (2, 20, 1), which indeed is nearly degenerate with (0, 32, 0) ($\Delta E \sim 2\ \mathrm{cm}^{-1}$). Because more than 10 quanta must be exchanged, however, the $(2, P-10-2v_3, v_3) \sim (0, P, 0)$ interpolyad coupling may not be sufficiently strong also to explain the large peak at $P = 42$. The level spectrum reveals that each of the states (0, 38, 0)–(0, 44, 0) is accompanied by an isomerization-type state, with the energy mismatch being smallest for $P = 42$ ($\Delta E \sim 10\ \mathrm{cm}^{-1}$). Because both kinds of states have highly excited bending character, the interpolyad coupling arising from diagonal bend anharmonicity is likely to be sufficiently strong to have a pronounced effect on the g_{22} value. Therefore, we believe that the unassigned isomerization states are responsible for the abrupt increase in the calculated g_{22} value at $v_2 = 38$.

The B-values are roughly an order of magnitude smaller than g_{22}, and therefore both anharmonic and Coriolis coupling effects must be taken into consideration. $B_{\mathrm{mech.}}$ shows a small maximum at $P = 42$, which must be due to an effect already contained in the $J = 0$ vibrational wave functions. However, this maximum is significantly enhanced for $B_{\mathrm{spec.}}$, i.e. when $\Delta K = \pm 1$ coupling is also taken into account. Actually, the (0, 38, 0)–(0, 44, 0) states with $K = 0$ are found also to be in near resonance with $K = 1$ isomerization-type states; the coupling between these two families of states must be of the Coriolis type. Thus, we tend to explain the large peak of $B_{\mathrm{spec.}}$ at $P = 42$ as a result of Coriolis coupling. This is supported by the fact that the experimental B and q_2 values show nearly identical behaviors; the latter constant, however, is exclusively sensitive to Coriolis coupling.

Whether these explanations for the maxima of the calculated g_{22} and $B_{\mathrm{spec.}}$ values are valid is unclear because of the unassignability of a large fraction of states in the high-energy $P \geq 36$ region. Moreover, whether the maxima in the measured constants have the same origins as the maxima in the calculated values is also not clear. Potential and dynamics calculations with accuracies higher than in the current study are required to unambiguously reveal all details of the SEP spectra.

CONCLUSIONS

This review of experimental and theoretical studies of the vibration-rotation spectrum and dynamics of HCP is intended as a case study in large-amplitude intramolecular motions. Encoded in the spectrum are qualitative changes in the quantum and classical dynamics and information about central topographic features of the PES, such as the minimum-energy isomerization path. A variety of computational approaches are shown to provide complementary information crucial to a global understanding of the spectrum and dynamics.

Exact quantum calculations, based on an accurate ab initio PES, provide wave functions, energy-level patterns, and computed quantities such as rotational constants. The nodal structures of wave functions, upon which rigorous eigenstate assignments are based, are not experimentally observable quantities. Spectroscopists must instead rely on energy-level patterns and effective Hamiltonian polyad models to assign the small observable subset of the totality of vibrational levels. The sudden appearance of large-amplitude bending isomerization states is predicted by both the exact PES calculations and the spectroscopic effective Hamiltonian model. Several well-understood qualitative changes in the spectrum—the appearance of large-B-value isomerization states, the sudden onset of spectroscopic perturbations, and abrupt resonance-like changes in vibrational fine-structure constants—are identified as universal signatures of qualitative changes in nodal patterns in wave functions, bifurcations in the forms of classical mechanical POs, and the emergence of new features in the reduced dimension semiclassical trajectories that correspond to intrapolyad dynamics.

This case study should serve as an introduction to the language, observables, and diagnostics of spectra, quantum calculations, classical POs, bifurcations, and reduced dimension semiclassical quantization. Workers in these closely related areas often have difficulty communicating with each other because they are unable to perceive the relationships between these complementary sets of observables, terminology, and analysis tools. HCP, by being the first triatomic molecule in which two different chemically bonded networks (HCP and HPC) can be simultaneously sampled by individual, spectroscopically observed eigenstates, and by having an ab initio PES characterized to near spectroscopic accuracy up to energies well above the bond rearrangement region, is the ideal molecule for such a case study.

ACKNOWLEDGMENTS

CB and RS thankfully acknowledge financial support by the Deutsche Forschungsgemeinschaft through the Sonderforschungsbereich 357 “Molekulare Mechanismen Unimolekularer Reaktionen” and by the Fonds der Chemischen Industrie. They are indebted to S Grebenshchikov and ME Kellman for invaluable discussions on the dynamics of HCP. RWF is grateful to the AFOSR for support under the grants No. F49620-94-1-0068 and -97-1-0040. HI thanks the Japan Society for the Promotion of Science for a postdoctoral fellowship at MIT; he is indebted to

Prof. N Mihami for his suggestion and support and to Mrs. C Nagao, for her assistance with experiments. SCF is grateful to the Humboldt Foundation for financial support.

LITERATURE CITED

1. Wilson EB, Decius JC, Cross PC. 1954. *Molecular Vibrations*. New York: McGraw-Hill
2. Dai H-L, Field RW, eds. 1995. *Molecular Dynamics and Spectroscopy by Stimulated Emission Pumping*. Singapore: World Sci.
3. Felker PM, Zewail AH. 1988. *Adv. Chem. Phys.* 70:265
4. Uzer T. 1991. *Phys. Rep.* 199:73
5. Lehmann KK, Scoles G, Pate BH. 1994. *Annu. Rev. Phys. Chem.* 45:241
6. Nesbitt DJ, Field RW. 1996. *J. Phys. Chem.* 100:12735
7. Wyatt RE, Zhang JZH, eds. 1996. *Dynamics of Molecules and Chemical Reactions*. New York: Dekker
8. Field RW, O'Brien JP, Jacobson MP, Solina SAB, Polik WF, Ishikawa H. 1997. *Adv. Chem. Phys.* 101:463
9. Gutzwiller MC. 1990. *Chaos in Classical and Quantum Mechanics*. New York: Springer
10. Blümel R, Reinhardt WP. 1997. *Chaos in Atomic Physics*. Cambridge, UK: Cambridge Univ. Press
11. Brody TA, Flores J, French JB, Mello PA, Pandey A, Wong SSM. 1981. *Rev. Mod. Phys.* 53:385
12. Zimmermann T, Cederbaum LS, Meyer H-D, Köppel H. 1987. *J. Phys. Chem.* 91:4446
13. Pique JP, Chen Y, Field RW, Kinsey JL. 1987. *Phys. Rev. Lett.* 58:475
14. Pique JP, Engel YM, Levine RD, Chen Y, Field RW, Kinsey JL. 1988. *J. Chem. Phys.* 88:5972
15. Hose G, Taylor HS. 1982. *J. Chem. Phys.* 76:5356
16. Lan BL, Bowman JM. 1993. *J. Phys. Chem.* 97:12535
17. Jonas DM, Rogaski CA, Wodtke AM, Yang X. 1995. See Ref. 2, pp. 513–61
18. Gallo MM, Hamilton TP, Schaefer HF III. 1990. *J. Am. Chem. Soc.* 112:8714
19. Hamilton CE, Kinsey JL, Field RW. 1986. *Annu. Rev. Phys. Chem.* 37:493
20. Northrup FJ, Sears TJ. 1992. *Annu. Rev. Phys. Chem.* 43:127
21. Papousek D, Aliev MR. 1982. *Molecular Vibrational-Rotational Spectra*. Amsterdam: Elsevier
22. Kellman ME. 1995. See Ref. 2, pp. 943–97
23. Keller H-M, Flöthmann H, Dobbyn AJ, Schinke R, Werner H-J, et al. 1996. *J. Chem. Phys.* 105:4983
24. Keller H-M, Schröder T, Stumpf M, Stöck C, Temps F, et al. 1997. *J. Chem. Phys.* 106:5359
25. Gomez Llorente JM, Pollak E. 1992. *Annu. Rev. Phys. Chem.* 43:91
26. Farantos SC. 1996. *Int. Rev. Phys. Chem.* 15:345
27. Heller EJ, Tomsovic S. 1993. *Phys. Today* 46(7):38
28. Child MS. 1991. *Semiclassical Mechanics with Molecular Applications*. Oxford, UK: Clarendon
29. Rose JP, Kellman ME. 1996. *J. Chem. Phys.* 105:7348
30. Keshavamurthy S, Ezra GS. 1997. *J. Chem. Phys.* 107:156
31. Bowman JM, Gazdy B. 1997. *J. Phys. Chem. A* 101:6384
32. Yang X, Rogaski CA, Wodtke AM. 1990. *J. Opt. Soc. Am. B* 7:1835
33. Jonas DM, Yang X, Wodtke AM. 1992. *J. Chem. Phys.* 97:2284
34. O'Keefe A, Deacon AG. 1988. *Rev. Sci. Instrum.* 59:2544

35. O'Brien JP, Jacobson MP, Sokol JJ, Coy SL, Field RW. 1998. *J. Chem. Phys.* 108: 7100
36. Ishikawa H, Nagao C, Mikami N, Field RW. 1998. *J. Chem. Phys.* 109:492
37. Lehmann KK, Ross SC, Lohr LL. 1985. *J. Chem. Phys.* 82:4460
38. Johns JWC, Shurvell HF, Tyler JK. 1969. *Can. J. Phys.* 47:893
39. Chen Y-T, Watt DM, Field RW, Lehmann KK. 1990. *J. Chem. Phys.* 93:2149
40. Ishikawa H, Chen Y-T, Ohshima Y, Wang J, Field RW. 1996. *J. Chem. Phys.* 105:7383
41. Farantos SC, Keller H-M, Schinke R, Yamashita Y, Morokuma K. 1996. *J. Chem. Phys.* 104:10055
42. Beck C, Keller H-M, Grebenschikov SY, Schinke R, Farantos SC, et al. 1997. *J. Chem. Phys.* 107:9818
43. Koput J. 1996. *Chem. Phys. Lett.* 263:401
44. Koput J, Carter S. 1997. *Spectrochim. Acta A* 53:1091
45. Puzzarini C, Tarroni R, Palmieri P, Demaison J, Senent ML. 1996. *J. Chem. Phys.* 105:3132
46. Beck C, Schinke R, Koput J. Submitted for publication
47. Jung M, Winnewisser BP, Winnewisser M. 1997. *J. Mol. Spectrosc.* 31:413
48. Schinke R. 1993. *Photodissociation Dynamics*. Cambridge, UK: Cambridge Univ. Press
49. Bačić Z, Light JC. 1989. *Annu. Rev. Phys. Chem.* 40:469
50. Cerjan C, ed. 1993. *Numerical Grid Methods and Their Applications to Schrödinger's Equation*. Dordrecht, The Netherlands: Kluwer Acad.
51. Lester WA Jr. 1976. In *Dynamics of Molecular Collisions*, ed. WH Miller, pp. 1-32. New York: Plenum
52. Tennyson J, Sutcliffe BT. 1982. *J. Chem. Phys.* 77:4061
53. Carter S, Handy NC. 1986. *Comp. Phys. Rep.* 5:117
54. Carrington T Jr. 1998. In *Encyclopedia of Computational Chemistry*, ed. P von Ragué Schleyer, NL Allinger, T Clark, J Gasteiger, PA Kollman, et al, 5:3157. Chichester, UK: Wiley

54a. Tennyson J, Miller S, Henderson JR. 1992. The calculation of highly excited vibration-rotation states of triatomic molecules. In *Methods in Computational Chemistry*. Vol. 4. *Molecular Vibrations*, ed. W Wilson, pp. 91–144. New York: Plenum

55. Bramley MJ, Carrington T Jr. 1993. *J. Chem. Phys.* 99:8519
56. Leforestier C, Wyatt RE. 1995. See Ref. 2, pp. 755–90
57. Wyatt RE, Iung C. 1996. In *Dynamics of Molecules and Chemical Reactions*, ed. RE Wyatt, JZH Zhang, pp. 59–121. New York: Dekker
58. Dobbyn AJ, Stumpf M, Keller H-M, Schinke R. 1995. *J. Chem. Phys.* 103:9947
59. Beck C, Schinke R, Koput J, Stamatiadis S, Farantos SC. Submitted for publication
60. Wall MR, Neuhauser D. 1995. *J. Chem. Phys.* 102:8011
61. Mandelshtam VA, Grozdanov TP, Taylor HS. 1995. *J. Chem. Phys.* 103:10074
62. Tennyson J, Henderson JR. 1989. *J. Chem. Phys.* 91:3815
63. Beck C. 1998. Theoretische Untersuchung zur Isomerisation von HCP im elektronischen Grundzustand. Doctoral thesis. Univ. Göttingen, Göttingen, Ger. 120 pp.
64. Svitak J, Li ZM, Rose J, Kellman ME. 1995. *J. Chem. Phys.* 102:4340
65. Joyeux M, Grebenshchikov SY, Schinke R. 1998. *J. Chem. Phys.* 109:8342
66. Ishikawa H, Nagao C, Mikami N, Field RW. 1997. *J. Chem. Phys.* 106:2980
67. Kellman ME. 1995. *Annu. Rev. Phys. Chem.* 46:395
68. Joyeux M. 1998. *J. Chem. Phys.* 109:2111
69. Nielsen HH. 1951. *Rev. Mod. Phys.* 23: 90
70. Bykov AD, Naumenko OV, Smirnov MA, Sinitsa LN, Brown LR, et al.1994. *Can. J. Phys.* 72:989
71. Pique JP, Joyeux M, Manners J, Sitja G. 1991. *J. Chem. Phys.* 95:8744

72. Delon A, Jost R. 1991. *J. Chem. Phys.* 95:5686
73. Yamanouchi K, Takeuchi S, Tsuchiya S. 1990. *J. Chem. Phys.* 92:4044
74. Quack M. 1990. *Annu. Rev. Phys. Chem.* 41:839
75. Lefebvre-Brion H, Field RW. 1986. *Perturbations in the Spectra of Diatomic Molecules*. Orlando, FL: Academic
76. Baer M, ed. 1985. *Theory of Chemical Reaction Dynamics*, Vol. 3. Boca Raton, FL: CRC.
77. Guckenheimer J, Holmes P. 1983. *Nonlinear Oscillations, Dynamical Systems, and Bifurcations of Vector Fields*. Berlin: Springer-Verlag
78. Taylor HS. 1995. See Ref. 2, pp. 1073–108
79. Heller EJ. 1984. *Phys. Rev. Lett.* 53:1515
80. Arranz FJ, Borondo F, Benito RM. 1998. *Eur. Phys. J. D* 4:181
81. Farantos SC. 1998. *Comput. Phys. Commun.* 108:240
82. Farantos SC. 1996. *Int. Rev. Phys. Chem.* 15:395
83. Contopoulos G. 1970. *Astron. J.* 75:96
84. Founargiotakis M, Farantos SC, Skokos H, Contopoulos G. 1997. *Chem. Phys. Lett.* 277:456
85. Contopoulos G, Farantos SC, Papadaki H, Polymilis C. 1994. *Phys. Rev. E* 50:4399
86. Prosmiti R, Farantos SC. 1995. *J. Chem. Phys.* 103:3299
87. Prosmiti R, Farantos SC, Guantes R, Borondo F, Benito RM. 1996. *J. Chem. Phys.* 104:2921
88. Prosmiti R, Farantos SC, Taylor HS. 1994. *Mol. Phys.* 82:1213
89. Maslov VP, Fedoriuk MV. 1981. *Semiclassical Approximations in Quantum Mechanics*. Dordrecht, Ger.: Deidel
90. Joyeux M, Sugny D, Tyng V, Kellman ME, Ishikawa H, et al. Submitted for publication
91. Birkhoff GD. 1966. *Dynamical Systems*. New York: AMS Colloq.
92. Gustavson FG. 1966. *Astron. J.* 71:670
93. Lu Z-M, Kellman ME. 1997. *J. Chem. Phys.* 107:1
94. Li ZM, Xiao L, Kellman ME. 1990. *J. Chem. Phys.* 92:2251
95. Joyeux M, Michaille L. 1997. *ACH Models Chem.* 134:573
96. Joyeux M. 1996. *Chem. Phys.* 203:281
97. Joyeux M. 1995. *Chem. Phys. Lett.* 247: 454
98. Ezra GS. 1996. *J. Chem. Phys.* 104:26
99. Jaffe C, Reinhardt WP. 1982. *J. Chem. Phys.* 77:5191
100. Shirts RB, Reinhardt WP. 1982. *J. Chem. Phys.* 77:5204
101. Mills IM. 1972. In *Molecular Spectroscopy: Modern Research*, ed. KN Rao, CW Mathews, pp. 115–40. New York: Academic